Author Manuscript

Author Manuscript

Author Manuscript

Author Manuscript

HHS Public Access

Author manuscript

Cell Rep. Author manuscript; available in PMC 2024 November 25.

Published in final edited form as:

Cell Rep. 2022 September 13; 40(11): 111321. doi:10.1016/j.celrep.2022.111321.

Human hepatocyte PNPLA3 148M exacerbates rapid non-alcoholic fatty liver disease development in chimeric mice

Mohammad Kabbani[1,2,*], **Eleftherios Michailidis**[1,*], **Sandra Steensels**[3], **Clifton G. Fulmer**[4,5], **Joseph M. Luna**[1], **Jérémie Le Pen**[1], **Matteo Tardelli**[3], **Brandon Razooky**[1], **Inna Ricardo-Lax**[1], **Chenhui Zou**[1,3], **Briana Zeck**[6], **Ansgar F. Stenzel**[1,7], **Corrine Quirk**[1], **Lander Foquet**[8], **Alison W. Ashbrook**[1], **William M. Schneider**[1], **Serkan Belkaya**[9], **Gadi Lalazar**[3,10], **Yupu Liang**[11], **Meredith Pittman**[4], **Lindsey Devisscher**[12], **Hiroshi Suemizu**[13], **Neil D. Theise**[6], **Luis Chiriboga**[6], **David E. Cohen**[3], **Robert Copenhaver**[8], **Markus Grompe**[8,14], **Philip Meuleman**[15], **Baran A. Ersoy**[3], **Charles M. Rice**[1], **Ype P. de Jong**[1,3,#]

[1]Laboratory of Virology and Infectious Disease, The Rockefeller University, New York, NY10065.

[2]Department of Gastroenterology, Hepatology and Endocrinology, Hannover Medical School, Hannover, Germany.

[3]Division of Gastroenterology and Hepatology, Weill Cornell Medicine, New York, NY10065.

[4]Department of Pathology, Weill Cornell Medicine, New York, NY10065.

[5]Robert J. Tomsich Pathology and Laboratory Medicine Institute, The Cleveland Clinic, Cleveland, Ohio, OH 44195.

[6]Department of Pathology, NYU Langone, New York, NY10028.

[7]Department of Infectious Diseases, Molecular Virology, Heidelberg University, Heidelberg, Germany.

[8]Yecuris Corporation, Tualatin, OR97062.

[9]St. Giles laboratory of Human Genetics of Infectious Diseases, The Rockefeller University, New York, NY10065.

[10]Laboratory of Cellular Biophysics, The Rockefeller University, New York, NY10065.

[11]Center for Clinical and Translational Science, The Rockefeller University, New York, NY10065.

[12]Department of Basic and Applied Medical Sciences, Gut-Liver Immunopharmacology Unit, Ghent University, Ghent, Belgium

Correspondence: Ype de Jong, Division of Gastroenterology and Hepatology, Weill Cornell Medicine, 413 East 69th Street, BB626, New York, NY 10021, Fax: 646-962-0355, ydj2001@med.cornell.edu.

*These authors contributed equally.

#Lead contact.

Author contributions:

MK, EM, SS, BAE and YPJ designed research; MK, EM, SS, CGF, JML, JLP, MT, BR, IRL, C.Z., BZ, AFS, CQ, LF, AWA, WMS, SB, GL, LC and YPJ performed experiments; MK, EM, SS, CGF, JML, JLP, MT, BR, IRL, CZ, BZ, AFS, CQ, LF, AWA, YL, DEC, MP, LD, MG, PM, BAE, CMR and YPJ analyzed data; HS, NDT and RC provided new reagents/analytic tools; DEC, PM, CMR and YPJ secured funding; MK, EM, and YPJ wrote the paper; YPJ directed the study.

Conflict of Interest Statement:

LF, RC and MG have financial interest in Yecuris corporation. The other authors have no conflict of interests to declare.

Author Manuscript Author Manuscript Author Manuscript Author Manuscript

[13]Central Institute for Experimental Animals, Kanagawa, Japan.

[14]Department of Pediatrics, Oregon Stem Cell Center, Oregon Health and Science University, Portland, OR97239.

[15]Laboratory of Liver Infectious Diseases, Ghent University, Ghent, Belgium.

Abstract

Advanced non-alcoholic fatty liver disease (NAFLD) is a rapidly emerging global health problem associated with pre-disposing genetic polymorphisms, most strikingly an isoleucine to methionine substitution in patatin-like phospholipase domain-containing protein 3 (PNPLA3-I148M). Here, we study how human hepatocytes with PNPLA3 148I and 148M variants engrafted in the livers of broadly immunodeficient chimeric mice respond to hypercaloric diets. As early as 4 weeks, mice developed dyslipidemia, impaired glucose tolerance, and steatosis with ballooning degeneration selectively in the human graft, followed by pericellular fibrosis after 8 weeks of hypercaloric feeding. Hepatocytes with the PNPLA3 148M variant, either from a homozygous 148M donor or overexpressed in a 148I donor background, developed microvesicular and severe steatosis with frequent ballooning degeneration, resulting in more active steatohepatitis than 148I hepatocytes. We conclude that PNPLA3 148M in human hepatocytes exacerbates NAFLD. These models will facilitate mechanistic studies into human genetic variant contributions to advanced fatty liver diseases.

Keywords

hypernutrition; NASH; human genetics; NAFLD progression

Introduction

Non-alcoholic fatty liver disease (NAFLD) has become the most prevalent liver disease in many countries, affecting approximately 25% of the world population.(Younossi et al., 2016) NAFLD is associated with obesity, insulin resistance, dyslipidemia and hypertension.(Yki-Järvinen, 2014) A subset of patients with NAFLD develop non-alcoholic steatohepatitis (NASH), which is widely believed to drive fibrosis progression towards advanced liver disease including cirrhosis and hepatocellular carcinoma (HCC) (Diehl and Day, 2017).

The complex nutritional and environmental factors leading to NAFLD remain to be better defined.(Buzzetti et al., 2016) In addition, a number of genetic variants have been associated with advanced NAFLD (Romeo et al., 2020). The first genetic polymorphism identified in a population with increased hepatic steatosis was rs738409 in patatin-like phospholipase domain containing protein-3 (*PNPLA3*) (Romeo et al., 2008). This polymorphism encodes for an isoleucine to methionine substitution at codon position 148 in PNPLA3. Since its identification by Hobbs and colleagues, the PNPLA3-I148M variant has been globally associated with advanced NAFLD and other liver diseases including HCC (Trépo et al., 2016).

Author Manuscript Author Manuscript Author Manuscript Author Manuscript

The mechanisms by which PNPLA3-148M drives advanced NAFLD remains an active area of investigation (Pingitore and Romeo, 2019; Tardelli et al., 2020). Although PNPLA3 is expressed in hepatocytes, hepatic stellate cells and adipocytes, accumulating evidence from mouse models indicates that hepatocyte-specific PNPLA3-148M promotes the pathogenesis of NAFLD. Transgenic overexpression of human PNPLA3-148M in mouse hepatocytes but not adipocytes exacerbated hepatic steatosis (Li et al., 2012). And while increased hepatic fat content was observed in *Pnpla3*-148M knock-in mice (Smagris et al., 2015), this was reversed by silencing *Pnpla3* in hepatocytes (Lindén et al., 2019). Functionally, PNPLA3 exhibits hydrolase activity towards triglycerides and acyltransferase activity for polyunsaturated fatty acids in phospholipids.(Pingitore and Romeo, 2019) PNPLA3-148M differs from 148I in several ways: PNPLA3-148M was shown to have decreased hydrolase activity against triglycerides (Huang et al., 2011), increased acyltransferase activity for lysophosphatidic acid (Kumari et al., 2012), resistance to ubiquitylation and proteasomal degradation (BasuRay et al., 2017), and inhibition of adipose triglyceride lipase on lipid droplets via interaction with α/β-hydrolase domain containing 5 (Wang et al., 2019; Yang et al., 2019). How these and other mechanistic differences drive NAFLD progression remains to be further elucidated.

Despite this vast disease burden there are no approved pharmacological therapies for NASH and sustained weight loss remains the only proven intervention. Given its complex pathogenesis, many different pathways are under pre-clinical and clinical investigation, some of which have resulted in compounds that progressed to Phase 3 trials (Wattacheril et al., 2018). Several of these pathways were identified in murine steatohepatitis models that share limited features with human disease (Farrell et al., 2019). Furthermore, investigational strategies that target subsets of NASH patients, e.g. those with genetic variants, are further complicated by species differences. In the case of PNPLA3, there is low sequence homology between the human and mouse orthologues. The human protein is 97 amino acids longer than the mouse PNPLA3. The relative mRNA expression starkly differs between adipose tissue and liver in each species (Huang et al., 2010; Lake et al., 2005) and it remains unclear if the same transcription factors regulate its expression in murine and human hepatocytes (Dubuquoy et al., 2011; Perttilä et al., 2012). Elucidation of the precise mechanisms by which human genetic variants in hepatocytes affect steatohepatitis would be aided by minimizing species-specific variances in a physiologically relevant experimental setting.

Here, we aimed to establish an animal model to study the role of human hepatocytes in NAFLD. We applied this model to study PNPLA3-148M, either from a 148M homozygous human hepatocyte donor and by overexpressing PNPLA3 variants in a 148I homozygous donor background. Our results show that human hepatocytes swiftly develop steatosis and ballooning degeneration in response to hypercaloric feeding and that NAFLD activity is higher when hepatocytes express PNPLA3-148M. These models will allow for mechanistic studies into human genetic variants implicated in advanced NAFLD.

Author Manuscript Author Manuscript Author Manuscript Author Manuscript

Results

Human hepatocytes in chimeric mice on Western diet rapidly develop steatosis

To investigate how the human graft in liver chimeric mouse models responds to a hypercaloric diet, we first created humanized mice by transplanting primary human hepatocytes (PHH) into preconditioned broadly immunodeficient *Fah*$^{-/-}$ NOD *Rag1*$^{-/-}$ *Il2rg*^{null} (FNRG) mice that lack T, B and NK cells as described previously(de Jong et al., 2014) (Michailidis et al., 2020). Cycling the protective drug nitisinone (Azuma et al., 2007) resulted in at least 50% humanization after which mice were subjected to an *ad libitum* Western-style diet (WD), which consists of 60% fat in diet and 10% sucrose in drinking water (Fig 1a). WD feeding did not result in graft loss as determined by persistently high (Billerbeck et al., 2016; Kawahara et al., 2010; Vanwolleghem et al., 2010) human serum albumin (hAlb) levels (Suppl Fig S1a). Periodic examination of huFNRG mouse livers showed steatosis(Yeh and Brunt, 2014) as early as 4 weeks on WD as evidenced by hematoxylin and eosin (H&E) staining (Fig 1b) and Oil Red O staining (Suppl Fig S1b). Steatosis almost exclusively affected the human graft whereas the remaining mouse hepatocytes, which appear larger with darker cytoplasm after H&E staining, rarely developed steatosis. The contrast in steatosis between mouse and human hepatocytes was further evident by using a human-specific marker (Fig 1c). Livers from highly humanized mice with severe steatosis showed sparing around periportal regions (Fig 1b), reminiscent of zonal steatosis in adult NAFLD patients. The zonal predominance was further highlighted by glutamine synthetase staining, which is mostly expressed in zone 3 hepatocytes (Fig 1d). In order to quantify steatosis in huFNRG mice, the human areas of chimeric livers were scored blindly according to clinical criteria (Yeh and Brunt, 2014). All animals developed mild to severe steatosis as early as 4 weeks on WD. Steatosis persisted for 20 weeks on WD, which contrasted with huFNRG mice on control chow (chow) that never developed more than 5% steatosis (Fig 1e). Clinical scoring was confirmed by total triacylglycerol (TAG) quantification in huFNRG livers, which was 7 to 11-fold higher in WD than chow mice (Fig 1f), and liver total cholesterol (Suppl Fig S1c). Overall, the accumulation of TAG in huFNRG livers correlated to the steatosis score of the human graft (Suppl Fig S1d). These findings show that human hepatocytes in huFNRG mice rapidly developed moderate steatosis in response to WD feeding.

We next tested if the marked steatosis difference between human and mouse hepatocytes was due to the NOD mouse background, the intermittent nitisinone used to protect *Fah*$^{-/-}$ mice from liver injury (Grompe et al., 1995), or the hepatocyte transplantation biology of the FNRG model. First, we subjected immunodeficient NOD *Rag1*$^{-/-}$ *Il2rg*^{null} (NRG) mice to WD feeding and nitisinone cycling. Even after 12 weeks on WD NRG livers developed minimal steatosis (Suppl Fig S1e), consistent with previous reports that T cell deficient mice are protected from experimental NAFLD (Bhattacharjee et al., 2014; Liu et al., 2015; Sun et al., 2018). To test if FNRG liver injury and/or hepatocyte repopulation physiology made hepatocytes susceptible to hypercaloric feeding we transplanted NRG mouse hepatocytes into FNRG mice. These animals were designated ‘murinized’ FNRG (muFNRG) mice. After 4 weeks on WD muFNRG livers did not display steatosis, but small areas of hepatocyte steatosis were present after 12 weeks of WD feeding (Fig 1g) which was in line with

Author Manuscript Author Manuscript Author Manuscript Author Manuscript

liver TAG levels (Suppl Fig S1f). These results show that human hepatocytes responded differently to WD feeding than mouse hepatocytes in these models.

We then tested if rapid steatosis was specific to this human hepatocyte donor (PHH1) and to the FNRG liver injury model, extending our protocols to other donors and liver chimeric mouse models. We first transplanted PHH2 into FNRG mice and equally immunodeficient thymidine kinase transgenic (TK-NOG) liver injury mice (Hasegawa et al., 2011). Despite reaching lower levels of humanization in both models, human hepatocyte islands developed steatosis in response to WD feeding but not on chow (Suppl Fig S1g). We also transplanted a third PHH donor (PHH3) into urokinase plasminogen activator (uPA)/SCID mice (Meuleman et al., 2005) that lack T and B cells and compared these to FNRG mice humanized with the same donor. Interestingly, humanized (hu-)uPA/SCID mice showed mild steatosis in the human graft on chow, which contrasted to the absence of steatosis in huFNRG livers on chow (Suppl Fig S1h). In the huFNRG model, PHH3 hepatocytes developed steatosis after 4 weeks of WD feeding. These data illustrate that humanized livers rapidly became steatotic following WD feeding regardless of the PHH donor, with different requirements for hypercaloric feeding between liver injury models.

Combined, these results demonstrate that human hepatocytes but not mouse hepatocytes in liver chimeric mice developed moderate steatosis as early as 4 weeks on WD.

Western diet affects systemic metabolic parameters of chimeric FNRG mice

NAFLD clinically overlaps with obesity, dyslipidemia, insulin resistance and possibly hypertension (Yki-Järvinen, 2014). To determine whether WD affects metabolic parameters in liver chimeras, we first measured body weight accumulation in adult huFNRG mice on an *ad libitum* WD or control chow (chow) diet. Compared to chow, WD caused nearly 20% increase in body weight within 4 weeks on the diet and maintained this difference through 12 weeks on WD (Fig 2a). Furthermore, the gonadal fat fraction (Fig 2b) increased 2- to 2.4-fold in huFNRG mice on WD compared to chow. These data demonstrate that WD feeding resulted in weight gain and gonadal fat accumulation in huFNRG mice.

We then tested plasma lipids in chimeric mice. Hepatocytes are central to lipid homeostasis, and humanized mice have plasma cholesterol profiles shifted toward lower density lipoproteins compared to wild type mice (Grompe and Strom, 2013). Similar to previous reports (Andreo et al., 2017; Bissig-Choisat et al., 2015; Minniti et al., 2020), huFNRG on chow contained more LDL than HDL cholesterol particles compared to muFNRG mice (Fig 2c). Four weeks of WD feeding resulted in stark increases in VLDL and LDL cholesterol in huFNRG plasma. Notably, the HDL fraction in huFNRG mice decreased with WD feeding whereas it rose in WD-fed muFNRG mice compared to chow (Suppl Fig S2a). Relative to chow, WD increased fasting serum triglycerides fractions, mostly in VLDL, and to a lesser extent in LDL fractions in huFNRG mice (Fig 2d, Suppl Fig S2b). These data show that WD feeding of huFNRG mice increased lower density lipoproteins and decreased HDL.

Given the strong clinical overlap between NAFLD and type 2 diabetes, we tested the effect of WD on glucose tolerance in huFNRG mice relative to muFNRG animals. While humanized animals started at a higher baseline, 4 weeks on WD resulted in a 2.2-fold

Author Manuscript Author Manuscript Author Manuscript Author Manuscript

increase in fasting blood glucose both in huFNRG and muFNRG mice (Fig 2e). Fasting mouse insulin levels on chow appeared higher in humanized than murinized FNRG animals, and increased only slightly in huFNRG animals after 4 weeks on WD (Fig 2f). To further characterize glucose metabolism, fasting animals were subjected to glucose, insulin or pyruvate tolerance tests. After 4 weeks on WD, huFNRG mice displayed severely impaired glucose clearance with 3.1-fold higher cumulative blood glucose than chow, whereas this difference was 1.67-fold higher in muFNRG mice (Fig 2g). By contrast huFNRG mice on WD remained responsive to insulin challenge (Fig 2g). To assess gluconeogenesis in these animals, a pyruvate injection after fasting for 16 hours resulted in a sharper rise in blood glucose in huFNRG on a WD than chow (Fig 2g). Eight weeks of WD feeding further prolonged time for glucose clearance in huFNRG mice (Suppl Fig S2c) without affecting endogenous insulin secretion (Suppl Fig S2d). These data show that WD feeding of chimeric FNRG mice affected glucose homeostasis without altering insulin-mediated glucose uptake.

Together these data show that WD in huFNRG mice causes increased body weight, dyslipidemia and impaired glucose metabolism compared to chow diet.

Western diet causes features of steatohepatitis with mild activity in huFNRG mice

Non-alcoholic steatohepatitis (NASH) frequently causes elevated serum transaminases(Ma et al., 2020) and is diagnosed histologically by the presence of hepatocyte ballooning and mononuclear infiltrates in the setting of >5% hepatocyte steatosis (Yeh and Brunt, 2014). Because the human graft rapidly developed steatosis, we tested whether huFNRG mice on WD also developed features associated with human NASH.

We quantified the activities of serum transaminases ALT and AST, which were elevated in huFNRG mice 4 weeks on WD compared to chow. With prolonged WD feeding, ALT activity remained high while AST increased further (Fig 3a). To determine whether the ALT was produced by human or mouse hepatocytes, human-specific ALT protein was quantified and this correlated with serum ALT activity (Suppl Fig S3a). The human origin of transaminase activity was further supported by the lack of ALT activity and only minimal increases in AST activity in muFNRG mice on WD (Suppl Fig S3b). These data show that WD increased human transaminases in huFNRG serum.

We next assessed whether human hepatocytes in huFNRG mice on WD displayed ballooning degeneration, a key characteristic of NASH (Yeh and Brunt, 2014). As early as 4 weeks on WD, steatotic hepatocytes in huFNRG mice showed ballooning degeneration that persisted for 20 weeks (Fig 3b–c, Suppl Fig S3c–d). Hepatocyte ballooning was specific to the human graft (Suppl Fig S3c) and not donor hepatocyte-specific (Suppl Fig S3e). The fraction of huFNRG mice with ballooning degeneration did not increase with prolonged WD feeding (Fig 3c) but rather positively associated with the severity of steatosis grade (Suppl Fig S3f). Ballooning degeneration, which remains less well-defined in mouse hepatocytes (Farrell *et al.*, 2019), was not observed in either NRG or muFNRG mice on WD. Another key feature of NASH is lobular inflammation, which is dominated by neutrophils and macrophages (Gadd et al., 2014). Despite their broad immunodeficient background inflammatory infiltrates were detected in a subset of huFNRG mouse livers after 4 weeks on WD (Fig 3b, Suppl Fig S3d), including an increasing number of hepatic macrophages

Author Manuscript Author Manuscript Author Manuscript Author Manuscript

on WD (Fig 3d), as well as neutrophils (Fig 3e). Lobular inflammation was observed in approximately one third of huFNRG mice up to 12 weeks on WD but was not observed at 20 weeks (Suppl Fig S3g). The livers of huFNRG mice on WD were scored according to the NAFLD activity score (NAS)(Kleiner et al., 2005) within the human graft. After 4 weeks on WD, 7 out of 8 huFNRG mice developed a NAS of 3 or more. Further durations of WD did not increase the fraction of mice with NAS ≥3 (Fig 3f). These data show that huFNRG mice developed steatosis and ballooning degeneration with infrequent lobular infiltrates following WD feeding.

Pericellular fibrosis can accompany NASH and is believed to result from ongoing steatohepatitis (Schuppan et al., 2018). To test if WD feeding of huFNRG mice caused fibrosis, livers were stained for collagen with Picrosirius Red (PSR). Pericellular collagen depositions were first observed in a few mice after 8 weeks on WD (Fig 3g), then in a larger fraction at 12 weeks and finally more prevalent after 20 weeks on WD (Fig 3h). Trichrome staining confirmed collagen depositions around human hepatocytes, which are smaller with paler cytoplasm compared to mouse hepatocytes (Suppl Fig S3h). Fibrosis was not PHH1 specific since mice humanized with donor PHH2 showed a similar phenotype after 10 weeks on WD (Suppl Fig S3i). These data indicate that prolonged WD feeding results in mild fibrosis around human hepatocytes.

Overall, these findings show that huFNRG mice developed features of steatohepatitis with borderline/mild activity as early as 4 weeks on WD, which was accompanied by pericellular fibrosis in the human graft after 8 weeks of WD feeding.

WD differentially affects human and mouse liver transcriptomes over time

In huFNRG chimeras that were created with PHH the non-parenchymal cells and leukocytes remained murine ((Billerbeck *et al.*, 2016) and unpublished observations). To determine how WD affected human and mouse gene expression we performed RNA-sequencing (RNA-seq) on livers from fasting huFNRG mice. STAR Alignment mapped >85% of transcripts uniquely to a human reference genome (Suppl Fig S4a).

Transcripts aligned to human genome (human reads) in mice that were fed WD for 4 weeks were compared to animals on chow, which identified 662 differentially expressed transcripts (Fig 4a). Among mice on WD human transcripts changed progressively less over time, totaling 154 at 8 vs. 4 weeks, 127 at 12 vs. 8 weeks, and 95 at 20 vs. 12 weeks (Fig 4a).

We then aligned transcripts of these highly humanized livers to mouse reference genome (mouse reads). In contrast, only 2 mouse transcripts were statistically different between huFNRG mice that were fed WD or chow for 4 weeks. Transcriptional changes in the mouse reads remained low for the first 12 weeks of WD feeding, but a large number of differentially expressed transcripts were observed by 20 weeks (Fig 4b).

To further investigate changes in the gene expression profile we performed gene ontology (GO) analysis using the GO, Kyoto Encyclopedia of Genes and Genomes (KEGG), REACTOME (REAC), and Transcription Factor (TF) databases. GO (Fig 4c), KEGG and REAC (Suppl Fig S4b) alignments of human reads revealed mostly downregulation of

Author Manuscript Author Manuscript Author Manuscript Author Manuscript

metabolic and catabolic pathways in mice 4 weeks on WD compared to chow, while transcription factors were upregulated (Suppl Fig S4b). A notable exception to many downregulated GO pathways was the Extracellular Matrix pathway, which was upregulated at 4 weeks of WD feeding. Comparing 8 vs. 4 weeks on WD identified upregulation of human GO pathways involved in cell death and NF-κB signaling. Later timepoints revealed fewer and statistically less significant pathways. Few mouse GO pathways were changed by WD feeding at early time points. At 20 weeks many pathways involved in cellular development and metabolism changed (Fig 4d, Suppl Fig S4c). Notably several metabolic pathways that were downregulated in the human transcriptome at 4 weeks were upregulated in the mouse transcriptome at 20 weeks.

Taken together, these data indicate that many metabolic pathways were transcriptionally downregulated in the human graft as early as 4 weeks on WD, while the mouse transcriptome of huFNRG mice remained largely silent until 20 weeks of WD feeding.

Mice humanized with a homozygous PNPLA3-148M donor develop steatohepatitis

Having established a new NAFLD model in chimeric mice, we set out to characterize how the PNPLA3-148M polymorphism in hepatocytes affected the phenotype. Thus far huFNRG mice were humanized with PHH donors that were homozygous for PNPLA3-148I (148I-huFNRG). We next tested how chimeric mice humanized with the PNPLA3-148M variant responded to WD. To this end broadly immunodeficient *Fah*$^{-/-}$ *Rag2*$^{-/-}$ *Il2rg*^{null} (FRG) mice (Azuma *et al.*, 2007) were humanized with a homozygous PNPLA3-148M donor (148M-huFRG) and given WD for 4 weeks. As expected WD caused metabolic changes, including raised fasting blood glucose, a minimal increase in fasting insulin and generally higher plasma triglycerides (Suppl Fig S5a–c). Livers of 148M-huFRG mice on WD had moderate (>33%) and severe (>66%) steatosis in contrast to <5% steatosis that was observed in chow-fed mice (Fig 5a–b). Histological findings were confirmed by 5.3-fold increase in TAG concentrations in the livers of 148M-huFRG mice on WD compared to chow-fed controls (Suppl Fig S5d). In contrast to previous 148I-huFNRG studies, the human graft showed not only macrovesicular but also microvesicular steatosis in all 148M-huFRG mice on WD (Fig 5c). In addition, 148M-huFRG livers contained Mallory-Denk bodies, high grade of ballooning degeneration and lobular inflammation, resulting in 4 out 5 mice with a NAS of 5 or above (Fig 5d, Suppl Fig S5e–f). FNRG mice that were humanized with the same 148M donor displayed a similar phenotype after WD feeding (Suppl Fig S5g). These data demonstrate that 148M-huFRG mice subjected to WD for 4 weeks showed features of steatohepatitis with moderate activity.

To investigate if 148M-huFRG mice transcriptionally responded differently to WD feeding than 148I-huFNRG animals, RNA-seq analyses was performed. The human graft in 148M-huFRG mice responded to 4 weeks on WD with numerous transcriptomic changes compared to chow, with 1458 downregulated and 1294 upregulated genes (Fig 5e). Pathway analyses revealed that metabolic and catabolic pathways were mostly downregulated by WD in 148M-huFRG mice, similar to previous results in 148I-huFNRG mice. Despite the similarities between both models, there were pathways, including oxidative phosphorylation and mitochondrial function, which were downregulated following WD only in the livers of

Author Manuscript Author Manuscript Author Manuscript Author Manuscript

148M-huFRG mice but not in 148I-huFNRG. In addition, some pathways were differentially upregulated by WD between these two models (Fig 5f). Comparing individual genes from livers of 148M-huFRG mice and 148I-huFNRG, there were 2329 differently expressed transcripts on chow and 3268 on WD (Suppl Fig S5h). However, when comparing transcripts that changed by WD feeding over chow in each model (Δ WD), there were only 108 genes differentially regulated between these models (Fig 5g).

Taken together, these findings show that 148M-huFRG mice developed microvesicular steatosis and steatohepatitis with moderate activity after 4 weeks on WD. While few pathways were transcriptionally different between 148M-huFRG and 148I-huFNRG mice on the same diet, several metabolic pathways were uniquely downregulated in 148M hepatocytes.

PNPLA3-148M overexpression in hepatocytes exacerbates steatosis in mice on WD

In addition to the PNPLA3 genotype, 148M-huFRG and 148I-huFNRG mice were distinct in human hepatocyte donor background and mouse strain differences. To better characterize if phenotypic differences were due to the PNPLA3 variant, we transduced mouse-passaged PHH cultures from a 148I homozygous donor (PHH1) with PNPLA3-148M and red fluorescent protein (RFP), 148I and RFP or RFP only before re-transplantation into mice (Michailidis *et al.*, 2020). Lentiviral transduction resulted in a dose-dependent increase in PNPLA3 protein *in vitro* prior to transplantation. Humanization kinetics did not differ between the PNPLA3 variants or RFP controls as determined by serum hAlb values (Suppl Fig S6a). Once hAlb serum levels plateaued, huFNRG mice with transduced PNPLA3-148M hepatocytes (td148M), td148I or tdRFP mice were subjected to 4 weeks on WD or chow (Fig 6a). In the WD groups lentiviral PNPLA3 transduction resulted in 61-fold higher mRNA levels compared to endogenous levels in tdRFP mice, while in the chow groups td148I had 2-fold higher levels than td148M mice. In tdRFP mice WD caused 3.7-fold higher endogenous PNPLA3 mRNA levels compared to chow (Suppl Fig S6b).

WD induced human hepatocyte steatosis in all three groups of mice, with only td148M livers containing widespread microvesicular steatosis (Fig 6b–c). Strikingly, even on chow td148M livers contained rare areas with human microvesicular steatosis, which was not observed in td148I or tdRFP livers (Suppl Fig S6c). Lipid quantification in livers from mice on WD showed 36% more triglycerides in td148M livers compared to td148I or tdRFP, with only minimal differences in mice on chow (Fig 6d). Despite these phenotypic changes, the NAS was not statistically different in td148M mice from td148I or tdRFP animals (Fig 6e, Suppl Fig 6d–e). These data demonstrate that PNPLA3 overexpressing huFNRG mice on WD developed steatohepatitis in the human graft, with td148M livers containing widespread microvesicular steatosis and increased hepatic triglycerides.

Since RNA-seq pathway analyses did not identify many differences between the 148M-huFRG and 148I-huFNRG models (Fig 5g), we performed qRT-PCR for 80 different human genes associated with fatty liver diseases. Liver tissue from td148I and td148M mice that were fed chow revealed 20 genes that were expressed differently, with lipoprotein lipase showing the greatest difference (Suppl Fig S6f). Comparing both groups following WD we identified only 8 genes that were affected by 2-fold or less, of which *CYP2E1* was most

Author Manuscript Author Manuscript Author Manuscript Author Manuscript

transcriptionally upregulated in td148M livers (Fig 6f). These results illustrate the modest expression differences between mice overexpressing the two PNPLA3 variants on WD.

Combined, these data show that PNPLA3-148M overexpression in hepatocytes on a homozygous 148I background caused widespread microvesicular steatosis and increased liver triglycerides after 4 weeks of WD feeding.

A high fat diet causes more active steatohepatitis in PNPLA3-148M overexpressing mice

We hypothesized that the minimal differences between tdRFP, td148I and td148M mice was caused by the severe steatosis phenotype of WD feeding in lentivirally transduced livers of huFNRG mice. Therefore, we challenged PNPLA3 overexpressing huFNRG mice with a high fat diet (HFD, 60% fat) only, excluding the sucrose drinking water portion of WD. After 4 weeks of HFD, PNPLA3-148M overexpression resulted in more steatosis (Fig 7a–b), which was confirmed by hepatic triglyceride quantification (Suppl Fig S7a). In td148M mice the HFD resulted in widespread microvesicular steatosis and Mallory Denk bodies (Fig 7c), which were not observed in either td148I or tdRFP mice. Ballooning degeneration in mice fed a HFD trended toward being more severe in the td148M group than in tdRFP and td148I ($p=0.063$, Suppl Fig S7b) while lobular inflammation was not affected by PNPLA3 overexpression (Suppl Fig S7c). Driven by steatosis and ballooning degeneration grades, the NAS was higher in td148M than in td148I or tdRFP mice (Fig 7d). These data show that HFD caused steatohepatitis in PNPLA3 transduced human grafts, with 148M transduction resulting in microvesicular steatosis, Mallory Denk bodies and higher activity compared to 148I.

PNPLA3 mRNA levels in liver pieces of td148I and td148M mice on HFD were similar (Suppl Fig S7d). Since lentiviral PHH transduction results in heterogeneous expression (Michailidis *et al.*, 2020) we next analyzed whether steatosis correlated to the transgene expression, using the RFP reporter as a surrogate marker (Kane et al., 2016). Low magnification fluorescence imaging of liver cross-sections stained for neutral lipids suggested that td148M livers on HFD contained more lipids than td148I mice (Fig 7e). At higher magnification steatosis appeared more severe in RFP positive areas of td148M livers whereas lipid distribution in td148I mice was not associated with RFP. We then analyzed RFP and neutral lipid intensity from individual small hepatocytes, calibrated to a highly humanized huFNRG mouse whose graft was severely steatotic (Suppl Fig S7e). Using all mice from an experiment with high hAlb serum values, a two-dimensional density plot of individual hepatocytes from three td148M animals showed that hepatocytes with higher RFP intensity contained more lipids, whereas lipids were equally distributed along RFP intensity in hepatocytes from four td148I mice (Fig 7f). These findings suggest that 148M but not 148I overexpression, as determined by a RFP reporter, exacerbated steatosis.

Combined, these findings show that PNPLA3-148M overexpression in hepatocytes from a homozygous 148I donor increased steatosis and steatohepatitis activity in chimeric mice on HFD.

Author Manuscript Author Manuscript Author Manuscript Author Manuscript

Discussion

In this study, we have established systems to model NAFLD genetics in human hepatocytes. The most striking phenotype in the 'standard' 148I-huFNRG model was the rapid onset of human steatosis on WD. This contrasted to the minimal steatosis in the residual mouse hepatocytes of huFNRG mice or in muFNRG controls. Both resembled immunodeficient non-humanized mouse models (Bhattacharjee *et al.*, 2014; Sun *et al.*, 2018) that require prolonged WD feeding to develop moderate steatosis (Ito et al., 2007). Xenograft models are limited by an unknown number of species-incompatible signaling pathways. Impaired crosstalk between human hepatocytes and murine cells likely contributed, as we previously showed for FGF15 and FGF19 signaling (Naugler et al., 2015), yet mouse and human hepatocytes may also inherently respond differently to overnutrition. This is supported by clinical observations of how rapidly hepatic fat content changes depending on the type and amount of food intake. For example, a three-week overfeeding study increased intrahepatic triglycerides up to 55% (Luukkonen et al., 2018) and a carbohydrate-restricted diet reduced hepatic fat by 44% in two weeks (Mardinoglu et al., 2018). These clinical data illustrate that hepatic steatosis dynamically responds to nutritional variations. HuFNRG mice can provide a platform to explore how hepatocytes rapidly respond to hypercaloric diets.

Hepatocytes are central to systemic lipid and glucose regulation. Similar to previous reports (Andreo *et al.*, 2017; Bissig-Choisat *et al.*, 2015; Minniti *et al.*, 2020) huFNRG on chow had starkly different lipid profiles than muFNRG, in part due to mice lacking cholesterol ester transfer protein (Minniti *et al.*, 2020). In addition, we show that fasting glucose and possibly fasting insulin levels were higher in huFNRG mice than muFNRG mice on chow. Species incompatibilities may contribute to the elevated fasting glucose of huFNRG mice on chow, as was illustrated by studies in the uPA liver chimeric model (Tateno et al., 2011). While some human donors develop spontaneous steatosis in these chimeras, similar to what we observed with PHH3, administration of human growth hormone reversed this phenotype, possibly through IGF-1 signaling in the liver (Tateno *et al.*, 2011; Yakar et al., 2004). We speculate that hepatocytes in huFNRG and TK-NOG mice are also predisposed to steatosis to varying degrees. These models only require a short duration of hypercaloric feeding to develop moderate steatosis in the human graft. Interestingly, muFNRG controls without hepatic steatosis developed glucose intolerance on WD that was proportionally similar to huFNRG mice with moderate steatosis. Uncoupling hepatocyte steatosis from glucose homeostasis in these models may advance insights into clinically distinct forms of NAFLD with and without insulin resistance (Luukkonen et al., 2016).

Despite their broad immunodeficiency huFNRG mice displayed the features that define human NASH, including ballooning degeneration, lobular infiltrates in a subset of animals, and pericellular fibrosis at later timepoints. This illustrates that several steatohepatitis features can be initiated in chimeric mice without lymphocytes or NK cells. In human NAFLD, portal immune infiltrates frequently contain lymphocytes whereas lobular infiltrates are dominated by macrophages and neutrophils (Gadd *et al.*, 2014; Guilliams et al., 2022). Emerging evidence suggests a role for parenchymal $CD8^+$ T cells in NASH, which are more abundant in patients with higher NAS and can be found in the proximity of ballooning hepatocytes (Ghazarian et al., 2017) (Dudek et al., 2021; Haas et al., 2019).

Author Manuscript Author Manuscript Author Manuscript Author Manuscript

In addition to $CD8^+$ T cells, livers from NASH patients contain higher percentages of Th17 cells (Rau et al., 2016) and B cells (Barrow et al., 2021). The contribution of these cell types to steatohepatitis progression and HCC formation have largely been defined in regular mouse NAFLD models (Cai et al., 2019; Kazankov et al., 2019; Sutti and Albano, 2020). With notable exceptions (Asgharpour et al., 2016) most mouse strains are resistant to steatohepatitis unless given choline-deficient diets or supraphysiological amounts of cholesterol (Farrell *et al.*, 2019). In such models there is ample evidence that lymphocytes contribute to steatohepatitis progression rather than protection. T and B cell deficient mice are resistant to NAFLD (Bhattacharjee *et al.*, 2014; Sun *et al.*, 2018). This may partially explain the lack of steatosis in our NRG and muFNRG controls, which were additionally treated with nitisinone, whose effect on steatosis remains to be defined. Elegant studies in mouse steatohepatitis models have shown pathogenic roles for B cells (Barrow *et al.*, 2021), Th17 cells (Gomes et al., 2016; Moreno-Fernandez et al., 2021) and $CD8^+$ T cells. Hepatic $CD8^+$ T cells contribute to NAFLD progression in a type I interferon dependent manner (Ghazarian *et al.*, 2017) and can become autoreactive (Sutti et al., 2014) in a steatohepatitis milieu where they contribute to hepatocyte loss, possibly through Fas-mediated killing (Dudek *et al.*, 2021). To what extent these pathways are functionally conserved between murine and human steatohepatitis will require immunocompetent humanized models and clinical studies. One experimental approach is to combine human immune system mice with liver chimeras (Billerbeck *et al.*, 2016; Wilson et al., 2014). These models could also become useful to investigate non-conserved pathways, e.g. IL-32 that lacks a mouse orthologue and was recently associated with advanced NAFLD (Baselli et al., 2020).

Transcriptomic characterization of huFNRG livers showed a large number of human metabolic pathways that were transcriptionally downregulated after 4 weeks of WD feeding and only a few pathways that were upregulated. Eight weeks of WD feeding caused upregulation of a small number of cellular stress and cell death pathways, and remarkably few human pathways transcriptionally changed after that. Equally surprising was the small number of mouse transcripts that changed during the first 12 weeks on WD. This may be partly explained by under-sampling of mouse hepatocytes particularly at earlier timepoints, as illustrated by changes in mouse metabolic pathways after 20 weeks WD when humanization histologically appeared to decline. In addition to undersampling of mouse tissues changes from WD in the mouse transcriptome may have been masked by cyclical nitisinone withdrawal and because non-parenchymal cells did not transcriptionally respond to signals from the human graft due to species incompatibilities. Elucidating these possibilities will require further studies, including in other chimera models without cyclical liver injury.

These systems will now allow for mechanistic studies into genetic variants that drive NAFLD. Many polymorphisms associated with elevated transaminases (Chambers et al., 2011) and most variants implicated in advanced NAFLD (Eslam et al., 2018) are in genes expressed in hepatocytes. As a proof-of-principle, we modeled the PNPLA3-148M polymorphism (Romeo *et al.*, 2008). Its prevalent allele frequency allowed for the identification of a high-quality homozygous 148M donor to create human chimeras. The comparison between the 148I and 148M PHH donors was limited by the additional genetic differences and because the mouse models were created at separate facilities. Different

Author Manuscript Author Manuscript Author Manuscript Author Manuscript

antibiotics were used at Rockefeller University and Yecuris to support survival during humanization, raising concerns over how microbiomes may have influenced the phenotypes. There are many associations between microbiome and human NAFLD(Aron-Wisnewsky et al., 2020; Kolodziejczyk et al., 2019), and murine fatty liver disease can be altered by fecal transplants (Barrow *et al.*, 2021; Yuan et al., 2019). Furthermore, PHH donors may carry their own microbiome.(Sookoian et al., 2020) It is therefore plausible that microbiome variation between models may have influenced some results in our study, including weight gain after stopping antibiotic treatment. We addressed some of these concerns by generating 148M homozygous huFNRG mice at Rockefeller University and by overexpressing both PNPLA3 variants in homozygous 148I hepatocytes. A limited number of 148M-huFNRG mice created at Rockefeller University phenocopied the mice created at Yecuris and only PNPLA3-148M overexpression resulted in microvesicular steatosis, suggesting that this phenotype in 148M-huFRG mice is associated with its PNPLA3 genotype. Differences between 148I and 148M had previously been identified in mouse hepatocytes and human cell lines (BasuRay *et al.*, 2017; Huang *et al.*, 2011; Li *et al.*, 2012; Luukkonen et al., 2019; Smagris *et al.*, 2015; Wang *et al.*, 2019), none of which displayed microvesicular steatosis. By contrast, hepatocytes in arguably the most physiological mouse model, namely in PNPLA3 148M knock-in mice, contained increased lipid droplet sizes on hypercaloric diet (Smagris *et al.*, 2015). This suggests that the microvesicular phenotype, which clinically correlates with advanced NASH (Tandra et al., 2011), may be a human-specific 148M hepatocyte response to hypernutrition.

Taken together these results show the utility of liver chimeras for studies of pathways that are genetically implicated in human fatty liver diseases. Notwithstanding their broad implications to advance human hepatocyte research, several technical challenges remain. Identifying high-quality PHH donors with rare allele variants, e.g. in *TM6SF2* or *MBOAT7* (Kozlitina et al., 2014; Mancina et al., 2016) will remain difficult. And creating isogenic controls for more frequent variants, e.g. in *PNPLA3* and *HSD17B13* (Abul-Husn et al., 2018), will require improvements in gene editing efficiency of primary human materials, either to disrupt genes or base edit polymorphisms (Anzalone et al., 2019). An alternative strategy is to base edit renewable cells such as pluripotent stem cells. However, hepatocyte-like cells derived from these sources have thus far failed to reliably and reproducibly humanize mouse chimera models (Chen et al., 2018; Luce et al., 2021). We here used an overexpression system to control for human hepatocyte donor differences. The lentiviral LTR promotor (Schoggins et al., 2011) in our models failed to recapitulate the complexities of dietary regulation of PNPLA3 transcription and translation (Huang *et al.*, 2010). This likely resulted in supraphysiological protein amounts particularly of the 148M variant with its known resistance to ubiquitylation (BasuRay *et al.*, 2017; Lindén *et al.*, 2019; Smagris *et al.*, 2015), and may explain the steatotic areas observed in some td148M mice on chow. Human and mouse PNPLA3 expression are regulated by sterol regulatory binding protein 1c (SREBP1c) (Dubuquoy *et al.*, 2011; Huang *et al.*, 2010; Perttilä *et al.*, 2012), while mouse *Pnpla3* transcription may additionally be under control of carbohydrate response element binding protein (ChREBP) (Dubuquoy *et al.*, 2011). Creating human liver chimeric mice with PNPLA3 expression under SREBP1c regulation would become a more physiological system to study PNPLA3-148M in hepatocytes with appropriate controls. Going forward,

Author Manuscript Author Manuscript Author Manuscript Author Manuscript

overcoming technical challenges with primary hepatocyte gene editing and hepatocyte-like cell engraftment would further advance the models presented here and generate ever more physiologically relevant systems to dissect the pathophysiology of genetic variants in human fatty liver diseases.

Limitations of the study:

The are several limitations to the studies presented here. Xenograft systems suffer from an unknown number of cross-species artifacts. In addition to known examples (e.g. FGF15/19, IGF-1) it must be assumed that many signaling pathways are altered and some pathways are non-functional. Because bulk RNA-seq was performed on random pieces of highly chimeric livers, mouse hepatocyte transcriptomic changes may have been undersampled, possibly resulting in false negative results. Another limitation of the study is that the xenograft models that were used in this study are based on broadly immunodeficient mice. The likely complex contributions of lymphocytes and NK cells to steatohepatitis severity and progression cannot be addressed in these models and may be one explanation why only a subset of 148I-huFNRG mice on hypercaloric diets showed a lobular infiltrate. Further limitations include the weight fluctuations from nitisinone cycling that is required for *Fah*−/− survival, which affected weight and may have influenced other metabolic responses. The lack of an NRG control group that did not receive nitisinone treatment. The study was underpowered to study PHH or mouse gender differences that are widely observed in wild type mice (Grove et al., 2010). The use of antibiotics during liver humanization likely caused lasting alterations of the microbiome that may have influenced the phenotypes in animals created in different facilities. And endotoxin nor other pathogen associated molecular pattern contaminants were quantified in the reagents used in this study, which may have influenced lentivirally transduced hepatocyte phenotypes.

STAR Methods

Resource Availability

Lead contact—Further information and requests for resources and reagents should be directed to and will be fulfilled by the lead contact, Ype de Jong (ydj2001@med.cornell.edu).

Materials availability—This study did not generate new unique reagents.

NRG mice are available from Jackson Labs.

FNRG mice can be requested from The Rockefeller University.

FRG mice can be obtained from Yecuris.

uPA/SCID mice can be requested from Ghent University

TK-NOG mice can be obtained from Taconics.

Data and code availability—Bulk RNA-seq data derived from mouse samples have been deposited at GEO and are publicly available as of the date of publication. Accession

Author Manuscript Author Manuscript Author Manuscript Author Manuscript

numbers are listed in the key resources table. The DOI is listed in the key resources table. Microscopy data reported in this paper will be shared by the lead contact upon request.

All original code has been deposited at Zenodo and is publicly available as of the date of publication. DOIs are listed in the key resources table.

Any additional information required to reanalyze the data reported in this paper is available from the lead contact upon request.

Experimental Model and subject details

Mice—Six to eight week old male and female *Fah*$^{-/-}$ NOD *Rag1*$^{-/-}$ *Il2rg*^{null} (FNRG) mice(de Jong *et al.*, 2014) were preconditioned with retrorsine(Michailidis *et al.*, 2020) and male *Fah*$^{-/-}$ *Rag2*$^{-/-}$ *Il2rg*$^{-/-}$ (FRG) mice(Azuma *et al.*, 2007) with adenoviral urokinase plasminogen activator (uPA) before transplantation with primary human hepatocytes (PHH). NOD *Rag1*$^{-/-}$ *Il2rg*^{null} (NRG) mice were obtained from Jackson Labs (Bar Harbor, ME) and received retrorsine and nitisinone cycling(de Jong *et al.*, 2014) similarly to FNRG mice. Seven week old male thymidine kinase transgenic mice on the NOD SCID *Il2rg*^{null} background (TK-NOG)(Hasegawa *et al.*, 2011) were obtained from Taconic Biosciences (Germantown, NY) and preconditioned with retrorsine(Michailidis *et al.*, 2020) and 48 hours 0.1mg/ml valganciclovir (Sigma, cat# PHR1626-1G) in drinking water 14 days prior to transplantation. Three week old male transgenic uPA$^{+/+}$/SCID mice were transplanted as previously described.(Meuleman *et al.*, 2005) The following PHH donors were used: cryopreserved or mouse-passaged (mp)PHH1 (HUM4188, Lonza), cryopreserved or mpPHH2 (HUM4129, Lonza), cryopreserved PHH3 (HFCP940, BD Biosciences) and cryopreserved PHH4 (HHF13022, Yecuris). Hepatocytes were genotyped only for the PNPLA3 rs734809 variant. Genotyping was performed by Sanger sequencing using forward 5'-GCCCTGCTCACTTGGAGAAA-3' and reverse primer 5'-TGAAAGGCAGTGAGGCATGG-3' as reported.(Santoro et al., 2010) To make PNPLA3 overexpressing mice, PNPLA3-148I or −148M (both containing the K434E variant(Donati et al., 2016)) were cloned into pSCRPSY(Schoggins *et al.*, 2011) (GenBank: KT368137.1) to generate VSVg pseudotyped lentiviral particles.(Michailidis *et al.*, 2020) Driven by HIV-LTR promoter, pSCRPSY allows a gene of interest (in our case either PNPLA3 variants or none in "tdRFP" controls) to be expressed from the completely spliced "early" HIV-1 mRNA, while TagRFP (a surrogate marker for transduction) is expressed from an unspliced late HIV-1 mRNA. (Kane *et al.*, 2016) mpPHH1 were isolated from huFNRG, plated in 6 well collagen-coated plates and transduced with pSCRPSY vectors by 1000g spinoculation. Three to 5 days after transduction ~5×10^5 cells/mouse were retransplanted into retrorsine preconditioned FNRG animals as described.(Michailidis *et al.*, 2020) Endotoxin levels were not quantified in the reagents. Mice were housed in a 12-hour light/dark cycle at 21°C and 50% humidity and were group housed of 3 to 5 mice. Littermates of the same sex were randomly assigned to experimental groups. All experiments were conducted under animal use protocols approved by Rockefeller University, Ghent University and Yecuris corporation. huFNRG and huTK-NOG mice were humanized at Rockefeller University, huFRG mice at Yecuris corporation and hu-uPA/SCID mice at Ghent University.

Author Manuscript Author Manuscript Author Manuscript Author Manuscript

Method details

Diet challenges—One week prior and during dietary studies, huFNRG, huFRG, NRG and muFNRG mice were changed from oral nitisinone (CuRx, Yecuris cat#20-0028) to intraperitoneal (i.p.) injections at 1mg/kg body weight for three days every 2 weeks. Injection solution was 0.5mg/ml nitisinone dissolved in 500mM $NaHCO_3$ pH 7.4 and diluted 1:10 in PBS−/− (Gibco, Thermo Fisher) to final concentration of 50μg/ml. During humanization or 'murinization' the FNRG, FRG and TK-NOG lines were maintained on an amoxicillin containing chow diet (modified PicoLab Mouse Diet 20, 5058 – 5B1Q, 0.12% Amoxicillin, irradiated; TestDiet, Richmond, IN) and autoclaved water. One week prior dietary challenge, amoxicillin medicated chow was replaced with regular chow diet (PicoLab Rodent Diet 20, 5053, irradiated; LabDiet, Fort Worth, TX) lacking amoxicillin. For High Fat Diet (HFD) studies, mice were given a diet with 60% kcal fat, 20% carbohydrates and 20% protein, with an estimated 0.03% w/w cholesterol fraction (D12492i irradiated; Research Diets, New Brunswick, NJ) and autoclaved water. For Western-style Diet (WD) studies, HFD was combined with 10% w/v sucrose (Fisher Scientific cat#S5-3; Fair Lawn, NJ) in autoclaved water. Sucrose drinking water was freshly made once a week. $uPA^{+/+}$/SCID mice were fed irradiated standard breeding chow (Mouse Breeding complete feed for mice (GE 16.7MJ/kg; 14.0 MJ/kg), Ssniff Spezialdiäten GmbH, Soest, Germany). All diets and drinking water were given *ad libitum*. Diet challenges in huFNRG, huFRG, NRG, muFNRG and huTK-NOG mice were done at Rockefeller University. Only huFNRG or huFRG mice with >70% human liver chimerism, determined by histology, were used for diet challenges.

Blood and tissue harvest—Serum was obtained from tail veins, retroorbital or submental venipuncture. Human albumin was serially quantified by ELISA sandwich method as previously described.(de Jong *et al.*, 2014) Briefly, flat bottom 96-well plates (Nunc, cat# 4424040) were coated with goat-anti-human-albumin antibodies (Bethyl, cat# A80-129A) with 50μl/well in 100mM bicarbonate buffer at 1:1000 dilutions. After washing three times with ELISA wash buffer (PBS with 0.05% Tween20), diluted mouse serum was incubated in coated ELISA plates for 90 min at 37°C while shaking. Hereafter, plates were washed three times with ELISA wash buffer and 50μl goat-anti-human-albumin HRP-conjugated antibody (Bethyl cat#A80-229P) were added in 1:5000 dilution. After 90 min incubation at 37°C while shaking, plates were washed five times with ELISA wash buffer and 75μl TMB (3,3',5,5'-tetramethylbenzidine, Sigma cat#T0440) was added to wells. After ca. 10 min of incubation at room temperature, development was stopped with 15μl 2N sulfuric acid. Absorbance was then measured within 30 min by a FLUOstar Omega - Microplate reader (BMG LABTECH, Germany) at 450nm.

Serum mouse insulin was quantified using Ultra-Sensitive Mouse Insulin ELISA Kit (Crystal Chem cat#90080, Elk Groove Village, IL) following manufacturer's instructions. In mice with hAlb serum levels >8mg/ml, ALT and AST activity (Elabscience cat#E-BC-K235 and K236, China), which is capable to detect mouse activity as per manufacturer, and human ALT protein (Abcam cat#ab234578) were determined following manufacturers instruction. Serum was obtained from submental venipuncture 2 to 3 days after last nitisinone injection cycle to minimize mouse transaminase activity. Tolerance tests to glucose (GTT), insulin

Author Manuscript Author Manuscript Author Manuscript Author Manuscript

(ITT) and pyruvate (PTT) were performed in FNRG mice in the weeks with no NTBC cycling injections similar as described.(Steensels et al., 2020) Briefly, age matched mice 4 to 12 weeks after dietary challenge with WD or chow were fasted with free access to water for 6 h prior to GTT and ITT and for 16 h prior to PTT. Approximately 5μl blood was collected from tail bleed before and at indicated intervals for up to 180 min following i.p. injection with 2.5 g/kg body weight glucose (Sigma Aldrich cat#G7021), 1 U/kg body weight human insulin analogue (Eli Lilly, Humulin R U-100), or 2 g/kg body weight pyruvate (Sigma Aldrich cat#P2256), each dissolved in isotonic PBS−/− (Gibco, Thermo Fisher Scientific). Blood glucose concentrations were determined using a GE100 Blood Glucose Monitor (GE, Ontario, CA). Prior to terminal blood and tissue collection (2 to 3 days after last nitisinone injection in $Fah^{-/-}$ strains), mice were fasted for 6 hours during light cycle with access to water. Blood was collected by submental and/or retroorbital venipuncture and tissue samples were weighed and stored in fixative or frozen on dry-ice and stored at −80°C. Blood was centrifuged with 16,000 × *g* for 15 min at 4°C and plasma was collected and stored at −80°C. Hepatic lipids were extracted from frozen liver tissue as described(Steensels *et al.*, 2020) and liver and plasma TG, total and free cholesterol were quantified according to manufacturer's instructions (Wako Diagnostics, Mountain View, CA). Equal volumes of plasma were pooled from three mice and lipoproteins were fractionated by fast protein liquid chromatography (ÄKTA pure FPLC system, GE Healthcare, Pittsburgh, PA, USA) and triglyceride and cholesterol in fractions quantified with reagent kits (Wako Diagnostics, Mountain View, CA).(Alves-Bezerra et al., 2019; Hyogo et al., 2002)

Liver histology and quantification—Neutral buffered formalin-fixed (Thermo Fisher Scientific cat#5725) paraffin-embedded liver samples were sectioned at 5μm onto charged slides (Fisher Scientific cat#22-042-924). Slides were dried for 1 hour at 60°C, deparaffinized in xylene, rehydrated through a graded series of ethanol, and rinsed in distilled water for 5 minutes. Sections were then stained with Hematoxylin (Richard-Allan Scientific cat #7211, USA) and Eosin (Leica cat#3801619) using our routine laboratory method described in [Carson, F.L., *Histotechnology: a self instructional text*. 2009, Chicago: ASCP Press., 114–123], and with Picro Sirius Red Stain (PSR) (Abcam cat#ab150681) and Masson's Trichrome (Newcomer Supply cat#9179A, USA) in accordance with manufacturer's supplied procedures. For chromogenic immunohistochemistry staining, unconjugated, polyclonal rabbit anti–Human Nuclear Mitotic Apparatus protein (Abcam Cat# 97585 Lot# GR268490 RRID AB_10680001),(Billerbeck *et al.*, 2016) unconjugated, mouse anti-Human Glutamine Synthetase (Ventana Medical Systems Lot# V0001337 RRID AB_2861318 clone GS-9)(Guilbert et al., 2020), monoclonal, anti-Mouse lymphocyte antigen 6 complex locus G6D (Ly-6G/6C) (Abcam Cat# 255, rat clone NIMP-R14, RRID AB_303154) [PMID:24428529], and monoclonal, anti-Mouse F4/80 (Cell Signaling Cat#70076, rabbit clone D2S9R, RRID AB_2799771) were used. Slides were scanned using a Leica Aperio AT2 System and digitally archived via eSlide Manager. To preserve lipids with and without fluorescent proteins for histopathological analysis, fresh liver samples haven been fixed in 4% paraformaldehyde (Electron Microscopy Sciences) for 18 hours, cryoprotected at 4°C with 10% and 18% sucrose w/v for 24 hours each before OCT (Sakura Finetek) embedding and storage at −80°C. OCT-embedded frozen specimens were cryosectioned at 5 μm onto charged slides (Fisher Scientific cat# 22-042-924).

Author Manuscript Author Manuscript Author Manuscript Author Manuscript

Slides were air-dried at room temperature overnight and fixed in 10% neutral buffered formalin for 1 hour at room temperature. Slides were then rinsed in distilled water, stained with BODIPY (Invitrogen cat# D3922) and Oil Red O (Sigma-Aldrich cat# O1391). For BODIPY staining, slides were incubated in Reaction Buffer (Ventana cat# 950-300) for 10 minutes and stained with BODIPY (1:1000 dilution) and DAPI (1:1000 dilution) in PBS for 60 minutes, and covered using ProLong™ Diamond Antifade Mountant (Invitrogen, cat# P36961). BODIPY, RFP, and DAPI were imaged on a Hamamatsu Nanozoomer 2.0 HT and digitally archived via SlidePath. For Oil Red O staining, sections were stained in Oil Red O solution for 10 minutes, rinsed with distilled water for 5 minutes, counterstained with hematoxylin (Richard-Allan Scientific cat# 7211,) for 1 minute and rinsed in distilled water for 1 minute. Samples were blued in 1.2% ammonium hydroxide solution for 1 minute, rinsed in distilled water for 1 minute, and coverslipped using a 50% glycerol solution. Slides were scanned using a Leica Aperio AT2 System and digitally archived via eSlide Manager. For fluorescence image analyses SVS image files derived from Hamamatsu Nanozoomer 2.0 HT were extracted and saved as uncompressed multiple 40x magnification tile images in TIFF format using FIJI (https://imagej.net/Fiji/Downloads)(Schindelin et al., 2012) and NDPITools plugin.(Deroulers et al., 2013) TIFF files of tile images were split into fluorescence channels (DAPI, BODIPY or RFP) and saved as 8-bit grayscale images. Masks were generated around human hepatocytes nuclei approximated by diameter size in DAPI images, enlarged three folds to approximate the size of human hepatocytes in chimeric livers and used for measuring BODIPY and RFP signal intensities. RFP and BODIPY intensities per approximated human hepatocyte were plotted as two-dimensional density plots using Python. Custom scripts used for the imaging analysis are publicly available at: https://doi.org/10.5281/zenodo.4531488. Histological scores were conducted from H&E stained samples by clinical pathologist (CF and MP), using the NAS system from NASH-CRN.(Kleiner *et al.*, 2005) Steatosis grade (0: <5%, 1: 5–33%, 2: >33–66% and 3:> 66%), lobular inflammation (0: no foci, 1: <2 foci / 200x field, 2: 2–4 foci, 3: >4 foci) and ballooning degeneration (0: none, 1: few ballooning cells, 2: many cells / prominent ballooning) were used to generate an overall score (NAS). Fibrosis staging was evaluated separately in PSR stained samples using the same system,(Kleiner *et al.*, 2005) with the following scores 0: none, 1: perisinusoidal or periportal, 1A: mild, zone 3, perisinusoidal, 1B: moderate, zone 3, perisinusoidal, 1C: portal/periportal.

Liver tissue transcriptional analyses—Around 25 mg of freshly harvested liver tissue was placed into 1ml 4°C TRIzol (Life Technologies, USA) with 500μl of 1mm glass beads (BioSpec Products cat# 11079110) and homogenized using MagNA lyser (Roche, USA), weighed and stored at −80°C. For RNA extraction, 500μl of liver/Trizol mixture was used for chloroform extraction using MaXtract™ (Qiagen, cat# 129056) and RNeasy® Mini Kit (Qiagen, cat# 74104) coupled with on-column DNaseI treatment (Qiagen cat#79254) following manufacturer's instructions. Extracted RNA was stored at −80°C. For qRT-PCR, cDNA was generated from liver RNA using SuperScript IV VILO (Thermo Fisher Scientific cat#11766050) following manufacturer's instructions. qRT-PCR was performed in 96-well Human Fatty Liver Array plates (Thermo Fisher Scientific cat # 4391524) on a QuantStudio 3 System (Applied Biosystem) for the following genes: *ABCA1, ACACA, ACADL, ACLY, ACOX1, ACSL5, ACSM3, ADIPOR1, ADIPOR2,*

Author Manuscript Author Manuscript Author Manuscript Author Manuscript

AKT1, APOA1, APOB, APOC3, APOE, ATP5C1, CASP3, CD36, CEBPB;CEBPB-AS1, CNBP, CPT1A, CPT2, CYP2E1, CYP7A1, DGAT2, FABP1, FABP3, FABP5, FAS, FASN, FOXA2, FOXO1, G6PC, G6PD, GCK, GK, GSK3B, HMGCR, HNF4A, IGF1, IGFBP1, IL1B, INSR, IRS1, LDLR, LEPR, LPL, MAPK1, MAPK8, MLXIPL, MTOR, NDUFB6, NFKB1, NR1H2, NR1H3, NR1H4, PCK2, PDK4, PIK3CA, PIK3R1, PKLR, PNPLA3, PPA1, PPARA, PPARG, PPARGC1A, PRKAA1, PTPN1, RBP4, RXRA, SCD, SERPINE1, SLC27A5, SLC2A1, SLC2A2, SLC2A4, SOCS3, SREBF1, SREBF2, STAT3, XBP1.

For bulk RNA sequencing (RNAseq) the quantity and integrity of extracted liver RNA were assessed using an Agilent 2100 Bioanalyzer (Agilent Technologies, Palo Alto, CA). Library construction and sequencing were performed by Novogene USA (Sacramento, CA), using Illumina S4 flowcell on Novaseq 6000 platform with a paired-end read length of 150 bp. The high-throughput sequencing data from this study have been submitted to the NCBI Sequence Read Archive (SRA) under accession number GSE166693

Quantification and statistical analysis

Number of samples used per time point and condition are described under “Experimental Model and subject details” section and in the legends of each associated figure along with statistical method used for analysis. Unless stated otherwise, statistical analyses were performed in GraphPad Prism (San Diego, Ca). Statistics are indicated in graphs if $p<0.05$.

Transcriptional changes in transduced mice livers were calculated over mean of the following housekeeping genes: *GAPDH, HPRT1, GUSB, ACTB, B2M, HMBS, IPO8, PGK1, RPLP0, TBP, TFRC*. Data were then analyzed and graphed in R (version 4.0.2).

Downstream RNAseq analysis was performed using a combination of programs. Alignments were parsed using STAR and differential expression was determined through limma/voom. (Ritchie et al., 2015) Alignments were parsed using STAR and differential expression was determined through limma/voom.(Ritchie *et al.*, 2015) GO, KEGG, REAC and TF enrichment were determined with the g:profiler R package.(Raudvere et al., 2019) Reference genome and gene model annotation files were downloaded from genome website browser (NCBI/UCSC/Ensembl) directly. Indices of the reference genome were built using STAR(Dobin et al., 2013) and paired-end clean reads were aligned to human or mouse reference genome using STAR (v2.5), setting the outFilterMismatchNmax argument to 2, from which gene level count tables were built using HTseq-count.(Anders et al., 2015) Gene-level read counts were then processed using the limma suite of tools(Ritchie *et al.*, 2015) first with a voom with quality weights transformation, followed by linear model fitting to determine differentially expressed genes. The P values for individual genes were adjusted using the Benjamini & Hochberg method. Corrected P-value of 0.05 and absolute foldchange of 1 were set as the threshold for significantly differential expression. Geneset testing on the entire dataset was performed using the camera() function to determine geneset direction using genesets extracted from MsigDB.(Liberzon et al., 2015) Select genesets were plotted as dotplots from the camera output. Gene Ontology (GO), Kyoto Encylopedia of Genes and Genomes (KEGG), and REACTOME database enrichment analysis of differentially expressed genes was further implemented with the g:profiler R

Author Manuscript Author Manuscript Author Manuscript Author Manuscript

package,(Raudvere *et al.*, 2019) in which gene length bias was corrected. Terms with corrected P-values less than 0.05 were considered significant.

Supplementary Material

Refer to Web version on PubMed Central for supplementary material.

Acknowledgements

This work was supported by the National Institutes of Health Grants R37DK048873, R01DK056626 and R01DK103046 (to DEC), R01DK085713 (to CMR), K08DK090576 and R01AA027327 (to YPJ) and the Starr Foundation (to CMR). PM was supported by grants from Ghent University (Special Research Fund – ICOH expert center) and the Research Foundation – Flanders (grants VirEOS 30981113 and G047417N). MK received funding from the Deutsche Forschungsgemeinschaft under grant number KA4688/1-1. The project was co-sponsored by the Center for Basic and Translational Research on Disorders of the Digestive System through the generosity of the Leona M. and Harry B. Helmsley Charitable trust (to EM). The NYULH Center for Biospecimen Research and Development, Histology and Immunohistochemistry Laboratory (RRID:SCR_018304) is supported in part by the Laura and Isaac Perlmutter Cancer Center Support Grant; NIH/NCI P30CA016087. The RU Center for Clinical and Translational Science Bioinformatics program is supported by the Clinical and Translational Award (CTSA) and the National Center for Advancing Translational Sciences (NCATS), part of the National Institutes of Health. We thank Branka Brukner Dabovic (NYULH – Department of Cell Biology Research) for help with imaging fluorescence samples. We thank the Rockefeller University High-Throughput, Bioimaging and Genomics Resource Centers.

References

Abul-Husn NS, Cheng X, Li AH, Xin Y, Schurmann C, Stevis P, Liu Y, Kozlitina J, Stender S, Wood GC, et al. (2018). A Protein-Truncating HSD17B13 Variant and Protection from Chronic Liver Disease. N Engl J Med 378, 1096–1106. 10.1056/NEJMoa1712191. [PubMed: 29562163]

Alves-Bezerra M, Li Y, Acuña M, Ivanova AA, Corey KE, Ortlund EA, and Cohen DE (2019). Thioesterase Superfamily Member 2 Promotes Hepatic VLDL Secretion by Channeling Fatty Acids Into Triglyceride Biosynthesis. Hepatology 70, 496–510. 10.1002/hep.30411. [PubMed: 30516845]

Anders S, Pyl PT, and Huber W (2015). HTSeq--a Python framework to work with high-throughput sequencing data. Bioinformatics 31, 166–169. 10.1093/bioinformatics/btu638. [PubMed: 25260700]

Andreo U, de Jong YP, Scull MA, Xiao JW, Vercauteren K, Quirk C, Mommersteeg MC, Bergaya S, Menon A, Fisher EA, and Rice CM (2017). Analysis of Hepatitis C Virus Particle Heterogeneity in Immunodeficient Human Liver Chimeric. Cell Mol Gastroenterol Hepatol 4, 405–417. 10.1016/j.jcmgh.2017.07.002. [PubMed: 28936471]

Anzalone AV, Randolph PB, Davis JR, Sousa AA, Koblan LW, Levy JM, Chen PJ, Wilson C, Newby GA, Raguram A, and Liu DR (2019). Search-and-replace genome editing without double-strand breaks or donor DNA. Nature 576, 149–157. 10.1038/s41586-019-1711-4. [PubMed: 31634902]

Aron-Wisnewsky J, Vigliotti C, Witjes J, Le P, Holleboom AG, Verheij J, Nieuwdorp M, and Clément K (2020). Gut microbiota and human NAFLD: disentangling microbial signatures from metabolic disorders. Nat Rev Gastroenterol Hepatol 17, 279–297. 10.1038/s41575-020-0269-9. [PubMed: 32152478]

Asgharpour A, Cazanave SC, Pacana T, Seneshaw M, Vincent R, Banini BA, Kumar DP, Daita K, Min HK, Mirshahi F, et al. (2016). A diet-induced animal model of non-alcoholic fatty liver disease and hepatocellular cancer. J Hepatol 65, 579–588. 10.1016/j.jhep.2016.05.005. [PubMed: 27261415]

Azuma H, Paulk N, Ranade A, Dorrell C, Al-Dhalimy M, Ellis E, Strom S, Kay MA, Finegold M, and Grompe M (2007). Robust expansion of human hepatocytes in Fah−/−/Rag2−/−/Il2rg−/− mice. Nat Biotechnol 25, 903–910. 10.1038/nbt1326. [PubMed: 17664939]

Barrow F, Khan S, Fredrickson G, Wang H, Dietsche K, Parthiban P, Robert S, Kaiser T, Winer S, Herman A, et al. (2021). Microbiota-Driven Activation of Intrahepatic B Cells Aggravates NASH Through Innate and Adaptive Signaling. Hepatology 74, 704–722. 10.1002/hep.31755. [PubMed: 33609303]

Baselli GA, Dongiovanni P, Rametta R, Meroni M, Pelusi S, Maggioni M, Badiali S, Pingitore P, Maurotti S, Montalcini T, et al. (2020). Liver transcriptomics highlights interleukin-32

Author Manuscript Author Manuscript Author Manuscript Author Manuscript

as novel NAFLD-related cytokine and candidate biomarker. Gut 69, 1855–1866. 10.1136/gutjnl-2019-319226. [PubMed: 32001554]

BasuRay S, Smagris E, Cohen JC, and Hobbs HH (2017). The PNPLA3 variant associated with fatty liver disease (I148M) accumulates on lipid droplets by evading ubiquitylation. Hepatology 66, 1111–1124. 10.1002/hep.29273. [PubMed: 28520213]

Bhattacharjee J, Kumar JM, Arindkar S, Das B, Pramod U, Juyal RC, Majumdar SS, and Nagarajan P (2014). Role of immunodeficient animal models in the development of fructose induced NAFLD. J Nutr Biochem 25, 219–226. 10.1016/j.jnutbio.2013.10.010. [PubMed: 24445047]

Billerbeck E, Mommersteeg MC, Shlomai A, Xiao JW, Andrus L, Bhatta A, Vercauteren K, Michailidis E, Dorner M, Krishnan A, et al. (2016). Humanized mice efficiently engrafted with fetal hepatoblasts and syngeneic immune cells develop human monocytes and NK cells. J Hepatol 65, 334–343. 10.1016/j.jhep.2016.04.022. [PubMed: 27151182]

Bissig-Choisat B, Wang L, Legras X, Saha PK, Chen L, Bell P, Pankowicz FP, Hill MC, Barzi M, Leyton CK, et al. (2015). Development and rescue of human familial hypercholesterolaemia in a xenograft mouse model. Nat Commun 6, 7339. 10.1038/ncomms8339. [PubMed: 26081744]

Buzzetti E, Pinzani M, and Tsochatzis EA (2016). The multiple-hit pathogenesis of non-alcoholic fatty liver disease (NAFLD). Metabolism 65, 1038–1048. 10.1016/j.metabol.2015.12.012. [PubMed: 26823198]

Cai J, Zhang XJ, and Li H (2019). The Role of Innate Immune Cells in Nonalcoholic Steatohepatitis. Hepatology 70, 1026–1037. 10.1002/hep.30506. [PubMed: 30653691]

Chambers JC, Zhang W, Sehmi J, Li X, Wass MN, Van der Harst P, Holm H, Sanna S, Kavousi M, Baumeister SE, et al. (2011). Genome-wide association study identifies loci influencing concentrations of liver enzymes in plasma. Nat Genet 43, 1131–1138. 10.1038/ng.970. [PubMed: 22001757]

Chen C, Soto-Gutierrez A, Baptista PM, and Spee B (2018). Biotechnology Challenges to In Vitro Maturation of Hepatic Stem Cells. Gastroenterology 154, 1258–1272. 10.1053/j.gastro.2018.01.066. [PubMed: 29428334]

de Jong YP, Dorner M, Mommersteeg MC, Xiao JW, Balazs AB, Robbins JB, Winer BY, Gerges S, Vega K, Labitt RN, et al. (2014). Broadly neutralizing antibodies abrogate established hepatitis C virus infection. Sci Transl Med 6, 254ra129. 10.1126/scitranslmed.3009512.

Deroulers C, Ameisen D, Badoual M, Gerin C, Granier A, and Lartaud M (2013). Analyzing huge pathology images with open source software. Diagn Pathol 8, 92. 10.1186/1746-1596-8-92. [PubMed: 23829479]

Diehl AM, and Day C (2017). Cause, Pathogenesis, and Treatment of Nonalcoholic Steatohepatitis. N Engl J Med 377, 2063–2072. 10.1056/NEJMra1503519. [PubMed: 29166236]

Dobin A, Davis CA, Schlesinger F, Drenkow J, Zaleski C, Jha S, Batut P, Chaisson M, and Gingeras TR (2013). STAR: ultrafast universal RNA-seq aligner. Bioinformatics 29, 15–21. 10.1093/bioinformatics/bts635. [PubMed: 23104886]

Donati B, Motta BM, Pingitore P, Meroni M, Pietrelli A, Alisi A, Petta S, Xing C, Dongiovanni P, del Menico B, et al. (2016). The rs2294918 E434K variant modulates patatin-like phospholipase domain-containing 3 expression and liver damage. Hepatology 63, 787–798. 10.1002/hep.28370. [PubMed: 26605757]

Dubuquoy C, Robichon C, Lasnier F, Langlois C, Dugail I, Foufelle F, Girard J, Burnol AF, Postic C, and Moldes M (2011). Distinct regulation of adiponutrin/PNPLA3 gene expression by the transcription factors ChREBP and SREBP1c in mouse and human hepatocytes. J Hepatol 55, 145–153. 10.1016/j.jhep.2010.10.024. [PubMed: 21145868]

Dudek M, Pfister D, Donakonda S, Filpe P, Schneider A, Laschinger M, Hartmann D, Hüser N, Meiser P, Bayerl F, et al. (2021). Auto-aggressive CXCR6. Nature 592, 444–449. 10.1038/s41586-021-03233-8. [PubMed: 33762736]

Eslam M, Valenti L, and Romeo S (2018). Genetics and epigenetics of NAFLD and NASH: Clinical impact. J Hepatol 68, 268–279. 10.1016/j.jhep.2017.09.003. [PubMed: 29122391]

Farrell G, Schattenberg JM, Leclercq I, Yeh MM, Goldin R, Teoh N, and Schuppan D (2019). Mouse Models of Nonalcoholic Steatohepatitis: Toward Optimization of Their Relevance to

Author Manuscript Author Manuscript Author Manuscript Author Manuscript

Human Nonalcoholic Steatohepatitis. Hepatology 69, 2241–2257. 10.1002/hep.30333. [PubMed: 30372785]

Gadd VL, Skoien R, Powell EE, Fagan KJ, Winterford C, Horsfall L, Irvine K, and Clouston AD (2014). The portal inflammatory infiltrate and ductular reaction in human nonalcoholic fatty liver disease. Hepatology 59, 1393–1405. 10.1002/hep.26937. [PubMed: 24254368]

Ghazarian M, Revelo XS, Nøhr MK, Luck H, Zeng K, Lei H, Tsai S, Schroer SA, Park YJ, Chng MHY, et al. (2017). Type I Interferon Responses Drive Intrahepatic T cells to Promote Metabolic Syndrome. Sci Immunol 2. 10.1126/sciimmunol.aai7616.

Gomes AL, Teijeiro A, Burén S, Tummala KS, Yilmaz M, Waisman A, Theurillat JP, Perna C, and Djouder N (2016). Metabolic Inflammation-Associated IL-17A Causes Non-alcoholic Steatohepatitis and Hepatocellular Carcinoma. Cancer Cell 30, 161–175. 10.1016/j.ccell.2016.05.020. [PubMed: 27411590]

Grompe M, Lindstedt S, al-Dhalimy M, Kennaway NG, Papaconstantinou J, Torres-Ramos CA, Ou CN, and Finegold M (1995). Pharmacological correction of neonatal lethal hepatic dysfunction in a murine model of hereditary tyrosinaemia type I. Nat Genet 10, 453–460. 10.1038/ng0895-453. [PubMed: 7545495]

Grompe M, and Strom S (2013). Mice with human livers. Gastroenterology 145, 1209–1214. 10.1053/j.gastro.2013.09.009. [PubMed: 24042096]

Grove KL, Fried SK, Greenberg AS, Xiao XQ, and Clegg DJ (2010). A microarray analysis of sexual dimorphism of adipose tissues in high-fat-diet-induced obese mice. Int J Obes (Lond) 34, 989–1000. 10.1038/ijo.2010.12. [PubMed: 20157318]

Guilbert MC, Therrien A, Soucy G, Trudel D, and Nguyen BN (2020). Nodular Regenerative Hyperplasia: Expression Pattern of Glutamine Synthetase and a Potential Role for Hepatic Progenitor Cells. Appl Immunohistochem Mol Morphol 28, 243–248. 10.1097/PAI.0000000000000793. [PubMed: 31335486]

Guilliams M, Bonnardel J, Haest B, Vanderborght B, Wagner C, Remmerie A, Bujko A, Martens L, Thoné T, Browaeys R, et al. (2022). Spatial proteogenomics reveals distinct and evolutionarily conserved hepatic macrophage niches. Cell 185, 379–396.e338. 10.1016/j.cell.2021.12.018. [PubMed: 35021063]

Haas JT, Vonghia L, Mogilenko DA, Verrijken A, Molendi-Coste O, Fleury S, Deprince A, Nikitin A, Woitrain E, Ducrocq-Geoffroy L, et al. (2019). Transcriptional Network Analysis Implicates Altered Hepatic Immune Function in NASH development and resolution. Nat Metab 1, 604–614. 10.1038/s42255-019-0076-1. [PubMed: 31701087]

Hasegawa M, Kawai K, Mitsui T, Taniguchi K, Monnai M, Wakui M, Ito M, Suematsu M, Peltz G, Nakamura M, and Suemizu H (2011). The reconstituted 'humanized liver' in TK-NOG mice is mature and functional. Biochem Biophys Res Commun 405, 405–410. 10.1016/j.bbrc.2011.01.042. [PubMed: 21238430]

Huang Y, Cohen JC, and Hobbs HH (2011). Expression and characterization of a PNPLA3 protein isoform (I148M) associated with nonalcoholic fatty liver disease. J Biol Chem 286, 37085–37093. 10.1074/jbc.M111.290114. [PubMed: 21878620]

Huang Y, He S, Li JZ, Seo YK, Osborne TF, Cohen JC, and Hobbs HH (2010). A feed-forward loop amplifies nutritional regulation of PNPLA3. Proc Natl Acad Sci U S A 107, 7892–7897. 10.1073/pnas.1003585107. [PubMed: 20385813]

Hyogo H, Roy S, Paigen B, and Cohen DE (2002). Leptin promotes biliary cholesterol elimination during weight loss in ob/ob mice by regulating the enterohepatic circulation of bile salts. J Biol Chem 277, 34117–34124. 10.1074/jbc.M203912200. [PubMed: 12114517]

Ito M, Suzuki J, Tsujioka S, Sasaki M, Gomori A, Shirakura T, Hirose H, Ishihara A, Iwaasa H, and Kanatani A (2007). Longitudinal analysis of murine steatohepatitis model induced by chronic exposure to high-fat diet. Hepatol Res 37, 50–57. 10.1111/j.1872-034X.2007.00008.x. [PubMed: 17300698]

Kane M, Zang TM, Rihn SJ, Zhang F, Kueck T, Alim M, Schoggins J, Rice CM, Wilson SJ, and Bieniasz PD (2016). Identification of Interferon-Stimulated Genes with Antiretroviral Activity. Cell Host Microbe 20, 392–405. 10.1016/j.chom.2016.08.005. [PubMed: 27631702]

Author Manuscript Author Manuscript Author Manuscript Author Manuscript

Kawahara T, Toso C, Douglas DN, Nourbakhsh M, Lewis JT, Tyrrell DL, Lund GA, Churchill TA, and Kneteman NM (2010). Factors affecting hepatocyte isolation, engraftment, and replication in an in vivo model. Liver Transpl 16, 974–982. 10.1002/lt.22099. [PubMed: 20677288]

Kazankov K, Jørgensen SMD, Thomsen KL, Møller HJ, Vilstrup H, George J, Schuppan D, and Grønbæk H (2019). The role of macrophages in nonalcoholic fatty liver disease and nonalcoholic steatohepatitis. Nat Rev Gastroenterol Hepatol 16, 145–159. 10.1038/s41575-018-0082-x. [PubMed: 30482910]

Kleiner DE, Brunt EM, Van Natta M, Behling C, Contos MJ, Cummings OW, Ferrell LD, Liu YC, Torbenson MS, Unalp-Arida A, et al. (2005). Design and validation of a histological scoring system for nonalcoholic fatty liver disease. Hepatology 41, 1313–1321. 10.1002/hep.20701. [PubMed: 15915461]

Kolodziejczyk AA, Zheng D, Shibolet O, and Elinav E (2019). The role of the microbiome in NAFLD and NASH. EMBO Mol Med 11. 10.15252/emmm.201809302.

Kozlitina J, Smagris E, Stender S, Nordestgaard BG, Zhou HH, Tybjærg-Hansen A, Vogt TF, Hobbs HH, and Cohen JC (2014). Exome-wide association study identifies a TM6SF2 variant that confers susceptibility to nonalcoholic fatty liver disease. Nat Genet 46, 352–356. 10.1038/ng.2901. [PubMed: 24531328]

Kumari M, Schoiswohl G, Chitraju C, Paar M, Cornaciu I, Rangrez AY, Wongsiriroj N, Nagy HM, Ivanova PT, Scott SA, et al. (2012). Adiponutrin functions as a nutritionally regulated lysophosphatidic acid acyltransferase. Cell Metab 15, 691–702. 10.1016/j.cmet.2012.04.008. [PubMed: 22560221]

Lake AC, Sun Y, Li JL, Kim JE, Johnson JW, Li D, Revett T, Shih HH, Liu W, Paulsen JE, and Gimeno RE (2005). Expression, regulation, and triglyceride hydrolase activity of Adiponutrin family members. J Lipid Res 46, 2477–2487. 10.1194/jlr.M500290-JLR200. [PubMed: 16150821]

Li JZ, Huang Y, Karaman R, Ivanova PT, Brown HA, Roddy T, Castro-Perez J, Cohen JC, and Hobbs HH (2012). Chronic overexpression of PNPLA3I148M in mouse liver causes hepatic steatosis. J Clin Invest 122, 4130–4144. 10.1172/JCI65179. [PubMed: 23023705]

Liberzon A, Birger C, Thorvaldsdóttir H, Ghandi M, Mesirov JP, and Tamayo P (2015). The Molecular Signatures Database (MSigDB) hallmark gene set collection. Cell Syst 1, 417–425. 10.1016/j.cels.2015.12.004. [PubMed: 26771021]

Lindén D, Ahnmark A, Pingitore P, Ciociola E, Ahlstedt I, Andréasson AC, Sasidharan K, Madeyski-Bengtson K, Zurek M, Mancina RM, et al. (2019). Pnpla3 silencing with antisense oligonucleotides ameliorates nonalcoholic steatohepatitis and fibrosis in Pnpla3 I148M knock-in mice. Mol Metab 22, 49–61. 10.1016/j.molmet.2019.01.013. [PubMed: 30772256]

Liu X, Huh JY, Gong H, Chamberland JP, Brinkoetter MT, Hamnvik OP, and Mantzoros CS (2015). Lack of mature lymphocytes results in obese but metabolically healthy mice when fed a high-fat diet. Int J Obes (Lond) 39, 1548–1557. 10.1038/ijo.2015.93. [PubMed: 25994806]

Luce E, Messina A, Duclos-Vallée JC, and Dubart-Kupperschmitt A (2021). Advanced techniques and awaited clinical applications for human pluripotent stem cell differentiation into hepatocytes. Hepatology. 10.1002/hep.31705.

Luukkonen PK, Nick A, Hölttä-Vuori M, Thiele C, Isokuortti E, Lallukka-Brück S, Zhou Y, Hakkarainen A, Lundbom N, Peltonen M, et al. (2019). Human PNPLA3-I148M variant increases hepatic retention of polyunsaturated fatty acids. JCI Insight 4. 10.1172/jci.insight.127902.

Luukkonen PK, Sädevirta S, Zhou Y, Kayser B, Ali A, Ahonen L, Lallukka S, Pelloux V, Gaggini M, Jian C, et al. (2018). Saturated Fat Is More Metabolically Harmful for the Human Liver Than Unsaturated Fat or Simple Sugars. Diabetes Care 41, 1732–1739. 10.2337/dc18-0071. [PubMed: 29844096]

Luukkonen PK, Zhou Y, Sädevirta S, Leivonen M, Arola J, Orešič M, Hyötyläinen T, and Yki-Järvinen H (2016). Hepatic ceramides dissociate steatosis and insulin resistance in patients with non-alcoholic fatty liver disease. J Hepatol 64, 1167–1175. 10.1016/j.jhep.2016.01.002. [PubMed: 26780287]

Ma X, Liu S, Zhang J, Dong M, Wang Y, Wang M, and Xin Y (2020). Proportion of NAFLD patients with normal ALT value in overall NAFLD patients: a systematic review and meta-analysis. BMC Gastroenterol 20, 10. 10.1186/s12876-020-1165-z. [PubMed: 31937252]

Author Manuscript Author Manuscript Author Manuscript Author Manuscript

Mancina RM, Dongiovanni P, Petta S, Pingitore P, Meroni M, Rametta R, Borén J, Montalcini T, Pujia A, Wiklund O, et al. (2016). The MBOAT7-TMC4 Variant rs641738 Increases Risk of Nonalcoholic Fatty Liver Disease in Individuals of European Descent. Gastroenterology 150, 1219–1230.e1216. 10.1053/j.gastro.2016.01.032. [PubMed: 26850495]

Mardinoglu A, Wu H, Bjornson E, Zhang C, Hakkarainen A, Räsänen SM, Lee S, Mancina RM, Bergentall M, Pietiläinen KH, et al. (2018). An Integrated Understanding of the Rapid Metabolic Benefits of a Carbohydrate-Restricted Diet on Hepatic Steatosis in Humans. Cell Metab 27, 559–571.e555. 10.1016/j.cmet.2018.01.005. [PubMed: 29456073]

Meuleman P, Libbrecht L, De Vos R, de Hemptinne B, Gevaert K, Vandekerckhove J, Roskams T, and Leroux-Roels G (2005). Morphological and biochemical characterization of a human liver in a uPA-SCID mouse chimera. Hepatology 41, 847–856. 10.1002/hep.20657. [PubMed: 15791625]

Michailidis E, Vercauteren K, Mancio-Silva L, Andrus L, Jahan C, Ricardo-Lax I, Zou C, Kabbani M, Park P, Quirk C, et al. (2020). Expansion, in vivo-ex vivo cycling, and genetic manipulation of primary human hepatocytes. Proc Natl Acad Sci U S A 117, 1678–1688. 10.1073/pnas.1919035117. [PubMed: 31915293]

Minniti ME, Pedrelli M, Vedin LL, Delbès AS, Denis RGP, Öörni K, Sala C, Pirazzini C, Thiagarajan D, Nurmi HJ, et al. (2020). Insights From Liver-Humanized Mice on Cholesterol Lipoprotein Metabolism and LXR-Agonist Pharmacodynamics in Humans. Hepatology 72, 656–670. 10.1002/hep.31052. [PubMed: 31785104]

Moreno-Fernandez ME, Giles DA, Oates JR, Chan CC, Damen MSMA, Doll JR, Stankiewicz TE, Chen X, Chetal K, Karns R, et al. (2021). PKM2-dependent metabolic skewing of hepatic Th17 cells regulates pathogenesis of non-alcoholic fatty liver disease. Cell Metab 33, 1187–1204.e1189. 10.1016/j.cmet.2021.04.018. [PubMed: 34004162]

Naugler WE, Tarlow BD, Fedorov LM, Taylor M, Pelz C, Li B, Darnell J, and Grompe M (2015). Fibroblast Growth Factor Signaling Controls Liver Size in Mice With Humanized Livers. Gastroenterology 149, 728–740.e715. 10.1053/j.gastro.2015.05.043. [PubMed: 26028580]

Perttilä J, Huaman-Samanez C, Caron S, Tanhuanpää K, Staels B, Yki-Järvinen H, and Olkkonen VM (2012). PNPLA3 is regulated by glucose in human hepatocytes, and its I148M mutant slows down triglyceride hydrolysis. Am J Physiol Endocrinol Metab 302, E1063–1069. 10.1152/ajpendo.00125.2011. [PubMed: 22338072]

Pingitore P, and Romeo S (2019). The role of PNPLA3 in health and disease. Biochim Biophys Acta Mol Cell Biol Lipids 1864, 900–906. 10.1016/j.bbalip.2018.06.018. [PubMed: 29935383]

Rau M, Schilling AK, Meertens J, Hering I, Weiss J, Jurowich C, Kudlich T, Hermanns HM, Bantel H, Beyersdorf N, and Geier A (2016). Progression from Nonalcoholic Fatty Liver to Nonalcoholic Steatohepatitis Is Marked by a Higher Frequency of Th17 Cells in the Liver and an Increased Th17/Resting Regulatory T Cell Ratio in Peripheral Blood and in the Liver. J Immunol 196, 97–105. 10.4049/jimmunol.1501175. [PubMed: 26621860]

Raudvere U, Kolberg L, Kuzmin I, Arak T, Adler P, Peterson H, and Vilo J (2019). g:Profiler: a web server for functional enrichment analysis and conversions of gene lists (2019 update). Nucleic Acids Res 47, W191–W198. 10.1093/nar/gkz369. [PubMed: 31066453]

Ritchie ME, Phipson B, Wu D, Hu Y, Law CW, Shi W, and Smyth GK (2015). limma powers differential expression analyses for RNA-sequencing and microarray studies. Nucleic Acids Res 43, e47. 10.1093/nar/gkv007. [PubMed: 25605792]

Romeo S, Kozlitina J, Xing C, Pertsemlidis A, Cox D, Pennacchio LA, Boerwinkle E, Cohen JC, and Hobbs HH (2008). Genetic variation in PNPLA3 confers susceptibility to nonalcoholic fatty liver disease. Nat Genet 40, 1461–1465. 10.1038/ng.257. [PubMed: 18820647]

Romeo S, Sanyal A, and Valenti L (2020). Leveraging Human Genetics to Identify Potential New Treatments for Fatty Liver Disease. Cell Metab 31, 35–45. 10.1016/j.cmet.2019.12.002. [PubMed: 31914377]

Santoro N, Kursawe R, D'Adamo E, Dykas DJ, Zhang CK, Bale AE, Calí AM, Narayan D, Shaw MM, Pierpont B, et al. (2010). A common variant in the patatin-like phospholipase 3 gene (PNPLA3) is associated with fatty liver disease in obese children and adolescents. Hepatology 52, 1281–1290. 10.1002/hep.23832. [PubMed: 20803499]

Author Manuscript Author Manuscript Author Manuscript Author Manuscript

Schindelin J, Arganda-Carreras I, Frise E, Kaynig V, Longair M, Pietzsch T, Preibisch S, Rueden C, Saalfeld S, Schmid B, et al. (2012). Fiji: an open-source platform for biological-image analysis. Nat Methods 9, 676–682. 10.1038/nmeth.2019. [PubMed: 22743772]

Schoggins JW, Wilson SJ, Panis M, Murphy MY, Jones CT, Bieniasz P, and Rice CM (2011). A diverse range of gene products are effectors of the type I interferon antiviral response. Nature 472, 481–485. 10.1038/nature09907. [PubMed: 21478870]

Schuppan D, Surabattula R, and Wang XY (2018). Determinants of fibrosis progression and regression in NASH. J Hepatol 68, 238–250. 10.1016/j.jhep.2017.11.012. [PubMed: 29154966]

Smagris E, BasuRay S, Li J, Huang Y, Lai KM, Gromada J, Cohen JC, and Hobbs HH (2015). Pnpla3I148M knockin mice accumulate PNPLA3 on lipid droplets and develop hepatic steatosis. Hepatology 61, 108–118. 10.1002/hep.27242. [PubMed: 24917523]

Sookoian S, Salatino A, Castaño GO, Landa MS, Fijalkowky C, Garaycoechea M, and Pirola CJ (2020). Intrahepatic bacterial metataxonomic signature in non-alcoholic fatty liver disease. Gut 69, 1483–1491. 10.1136/gutjnl-2019-318811. [PubMed: 31900291]

Steensels S, Qiao J, Zhang Y, Maner-Smith KM, Kika N, Holman CD, Corey KE, Bracken WC, Ortlund EA, and Ersoy BA (2020). Acot9 traffics mitochondrial short-chain fatty acids towards de novo lipogenesis and glucose production in the liver. Hepatology. 10.1002/hep.31409.

Sun G, Jin H, Zhang C, Meng H, Zhao X, Wei D, Ou X, Wang Q, Li S, Wang T, et al. (2018). OX40 Regulates Both Innate and Adaptive Immunity and Promotes Nonalcoholic Steatohepatitis. Cell Rep 25, 3786–3799.e3784. 10.1016/j.celrep.2018.12.006. [PubMed: 30590049]

Sutti S, and Albano E (2020). Adaptive immunity: an emerging player in the progression of NAFLD. Nat Rev Gastroenterol Hepatol 17, 81–92. 10.1038/s41575-019-0210-2. [PubMed: 31605031]

Sutti S, Jindal A, Locatelli I, Vacchiano M, Gigliotti L, Bozzola C, and Albano E (2014). Adaptive immune responses triggered by oxidative stress contribute to hepatic inflammation in NASH. Hepatology 59, 886–897. 10.1002/hep.26749. [PubMed: 24115128]

Tandra S, Yeh MM, Brunt EM, Vuppalanchi R, Cummings OW, Ünalp-Arida A, Wilson LA, and Chalasani N (2011). Presence and significance of microvesicular steatosis in nonalcoholic fatty liver disease. J Hepatol 55, 654–659. 10.1016/j.jhep.2010.11.021. [PubMed: 21172393]

Tardelli M, Bruschi FV, and Trauner M (2020). The role of metabolic lipases in the pathogenesis and management of liver disease. Hepatology. 10.1002/hep.31250.

Tateno C, Kataoka M, Utoh R, Tachibana A, Itamoto T, Asahara T, Miya F, Tsunoda T, and Yoshizato K (2011). Growth hormone-dependent pathogenesis of human hepatic steatosis in a novel mouse model bearing a human hepatocyte-repopulated liver. Endocrinology 152, 1479–1491. 10.1210/en.2010-0953. [PubMed: 21303949]

Trépo E, Romeo S, Zucman-Rossi J, and Nahon P (2016). PNPLA3 gene in liver diseases. J Hepatol 65, 399–412. 10.1016/j.jhep.2016.03.011. [PubMed: 27038645]

Vanwolleghem T, Libbrecht L, Hansen BE, Desombere I, Roskams T, Meuleman P, and Leroux-Roels G (2010). Factors determining successful engraftment of hepatocytes and susceptibility to hepatitis B and C virus infection in uPA-SCID mice. J Hepatol 53, 468–476. 10.1016/j.jhep.2010.03.024. [PubMed: 20591528]

Wang Y, Kory N, BasuRay S, Cohen JC, and Hobbs HH (2019). PNPLA3, CGI-58, and Inhibition of Hepatic Triglyceride Hydrolysis in Mice. Hepatology 69, 2427–2441. 10.1002/hep.30583. [PubMed: 30802989]

Wattacheril J, Issa D, and Sanyal A (2018). Nonalcoholic Steatohepatitis (NASH) and Hepatic Fibrosis: Emerging Therapies. Annu Rev Pharmacol Toxicol 58, 649–662. 10.1146/annurev-pharmtox-010617-052545. [PubMed: 29058997]

Wilson EM, Bial J, Tarlow B, Bial G, Jensen B, Greiner DL, Brehm MA, and Grompe M (2014). Extensive double humanization of both liver and hematopoiesis in FRGN mice. Stem Cell Res 13, 404–412. 10.1016/j.scr.2014.08.006. [PubMed: 25310256]

Yakar S, Setser J, Zhao H, Stannard B, Haluzik M, Glatt V, Bouxsein ML, Kopchick JJ, and LeRoith D (2004). Inhibition of growth hormone action improves insulin sensitivity in liver IGF-1-deficient mice. J Clin Invest 113, 96–105. 10.1172/JCI17763. [PubMed: 14702113]

Author Manuscript Author Manuscript Author Manuscript Author Manuscript

Yang A, Mottillo EP, Mladenovic-Lucas L, Zhou L, and Granneman JG (2019). Dynamic interactions of ABHD5 with PNPLA3 regulate triacylglycerol metabolism in brown adipocytes. Nat Metab 1, 560–569. 10.1038/s42255-019-0066-3. [PubMed: 31497752]

Yeh MM, and Brunt EM (2014). Pathological features of fatty liver disease. Gastroenterology 147, 754–764. 10.1053/j.gastro.2014.07.056. [PubMed: 25109884]

Yki-Järvinen H (2014). Non-alcoholic fatty liver disease as a cause and a consequence of metabolic syndrome. Lancet Diabetes Endocrinol 2, 901–910. 10.1016/S2213-8587(14)70032-4. [PubMed: 24731669]

Younossi ZM, Koenig AB, Abdelatif D, Fazel Y, Henry L, and Wymer M (2016). Global epidemiology of nonalcoholic fatty liver disease-Meta-analytic assessment of prevalence, incidence, and outcomes. Hepatology 64, 73–84. 10.1002/hep.28431. [PubMed: 26707365]

Yuan J, Chen C, Cui J, Lu J, Yan C, Wei X, Zhao X, Li N, Li S, Xue G, et al. (2019). Fatty Liver Disease Caused by High-Alcohol-Producing Klebsiella pneumoniae. Cell Metab 30, 675–688.e677. 10.1016/j.cmet.2019.08.018. [PubMed: 31543403]

Author Manuscript Author Manuscript Author Manuscript Author Manuscript

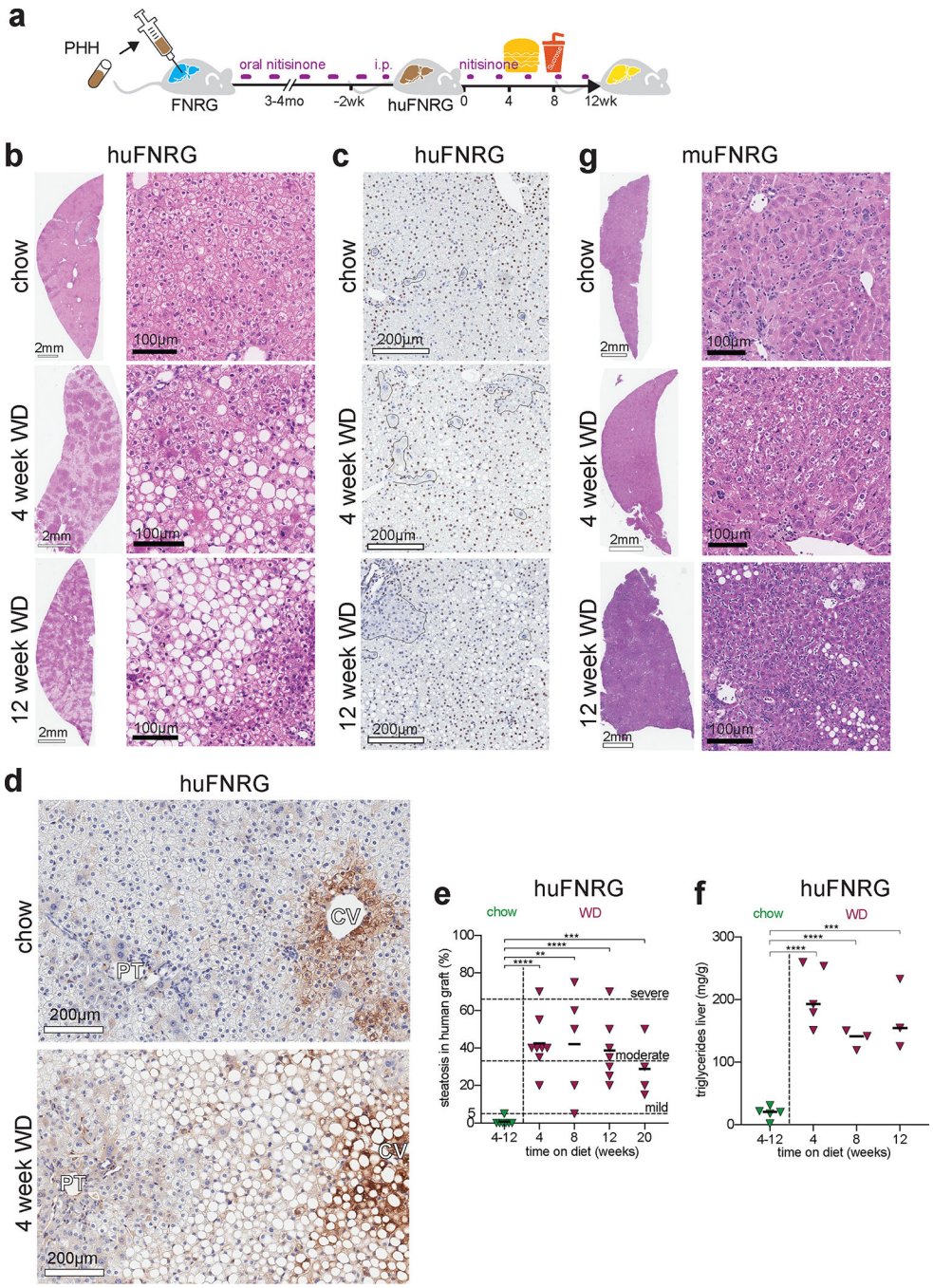

Figure 1: Human hepatocytes in chimeric mice on WD rapidly develop steatosis.

a) Experimental timeline of FNRG mice that were transplanted with primary human hepatocytes (PHH), cycled off nitisinone to create huFNRG mice, and then subjected to chow or WD for up to 12 weeks.

b) H&E staining on livers from huFNRG mice on chow and after 4 or 12 weeks on WD.

c) Staining against human nuclear mitotic apparatus-1 in livers of huFNRG mice on chow and 4 or 12 weeks on WD. Areas with predominantly mouse hepatocytes are outlined.

Author Manuscript Author Manuscript Author Manuscript Author Manuscript

d) Staining against human glutamine synthetase on livers from huFNRG mice on chow and 4 weeks on WD. Central vein (CV), portal tract (PT).

e) Liver steatosis score of the human graft in huFNRG mice on chow and after 4 to 20 weeks on WD. Symbols individual mice, bars are median, unpaired *t*-test with **p<0.005, ***p<0.0005 and ****p<0.0001.

f) Hepatic triglyceride levels in livers of huFNRG mice on chow and after 4 to 12 weeks on WD. Symbols individual mice, bars are median, unpaired *t*-test with ***p<0.0005 and ****p<0.0001.

g) H&E staining on livers from muFNRG mice on chow and after 4 or 12 weeks on WD.

Author Manuscript Author Manuscript Author Manuscript Author Manuscript

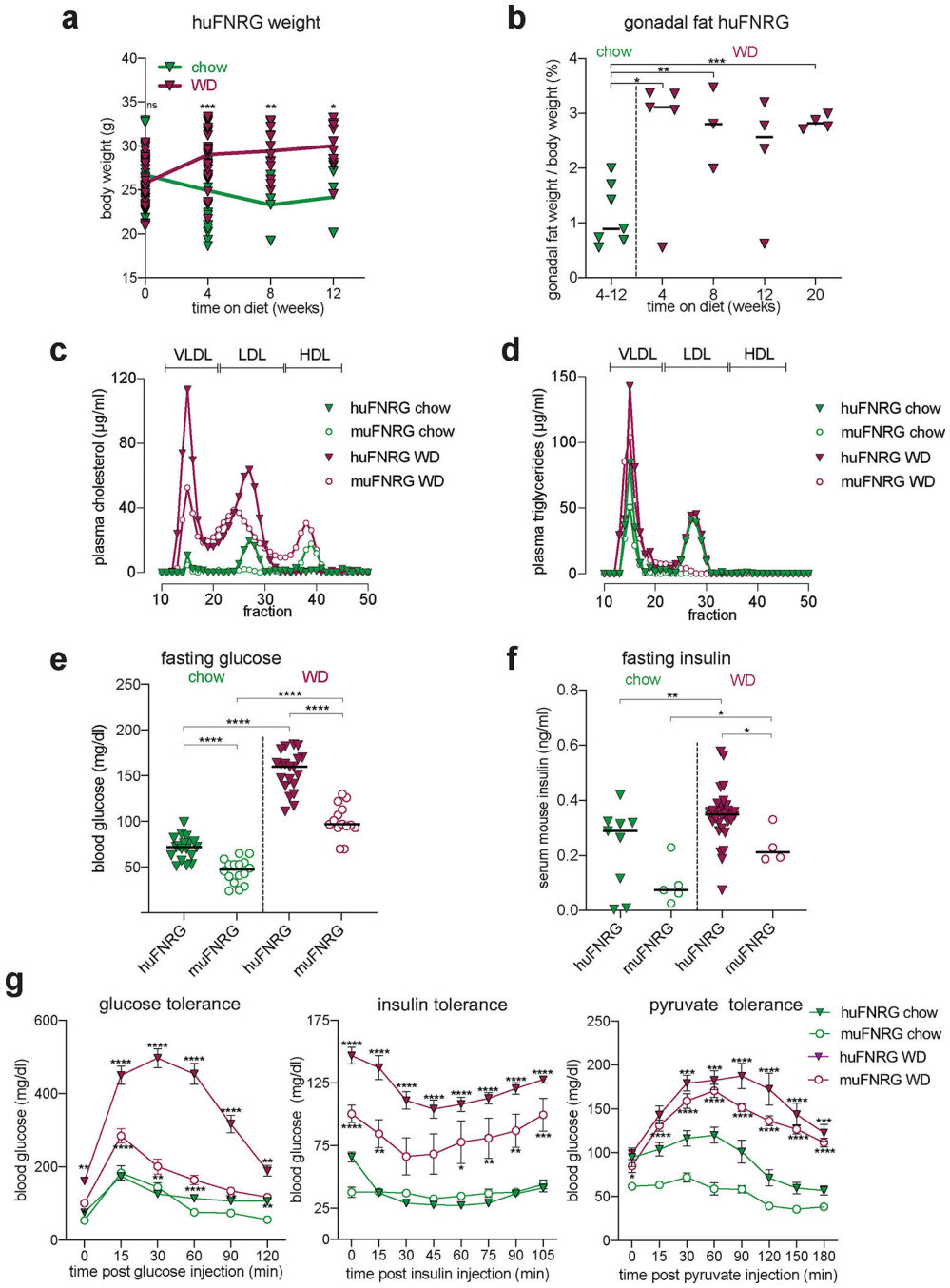

Figure 2: Systemic metabolic effects of WD in chimeric FNRG mice.

a) Body weight in huFNRG mice during time course of chow or WD feeding. Symbols individual mice, line is mean, two-way ANOVA Sidak pairwise comparison *p<0.05, **p<0.005, ***p<0.0005.

b) Gonadal fat fraction of total body weight in huFNRG mice on chow and after 4 to 20 weeks on WD. Symbols individual mice, bars are median, unpaired *t*-test with *p<0.05, **p<0.005, ***p<0.0005.

Author Manuscript Author Manuscript Author Manuscript Author Manuscript

c) Cholesterol in plasma lipoprotein fractions from huFNRG and muFNRG mice on chow and after 4 weeks on WD. Pooled plasma (3 mice/group), symbols are technical means.
d) Triglycerides in plasma lipoprotein fractions from huFNRG and muFNRG mice on chow and after 4 weeks on WD. Pooled plasma (3 mice/group), symbols are technical means.
e) Fasting blood glucose from huFNRG and muFNRG mice on chow and after 4 weeks on WD. Symbols individual mice, lines are median, unpaired *t*-test ****p<0.0001.
f) Fasting serum mouse insulin from huFNRG and muFNRG mice on chow and after 4 weeks on WD. Symbols individual mice, lines are median, unpaired *t*-test with *p<0.05, **p<0.005.
g) Intraperitoneal glucose, insulin and pyruvate tolerance testing in huFNRG and muFNRG mice on chow and after 4 weeks on WD. Blood glucose values measured at baseline (0) and at indicated timepoints after i.p. injections with each agent. Symbols are mean ± SEM of 5–7 mice per group, two-way ANOVA Sidak pairwise comparison of huFNRG on chow and WD (p-values on top) or muFNRG on chow and WD (p-values in bottom), *p<0.05, **p<0.005, ***p<0.0005 and ****p<0.0001

Author Manuscript Author Manuscript Author Manuscript Author Manuscript

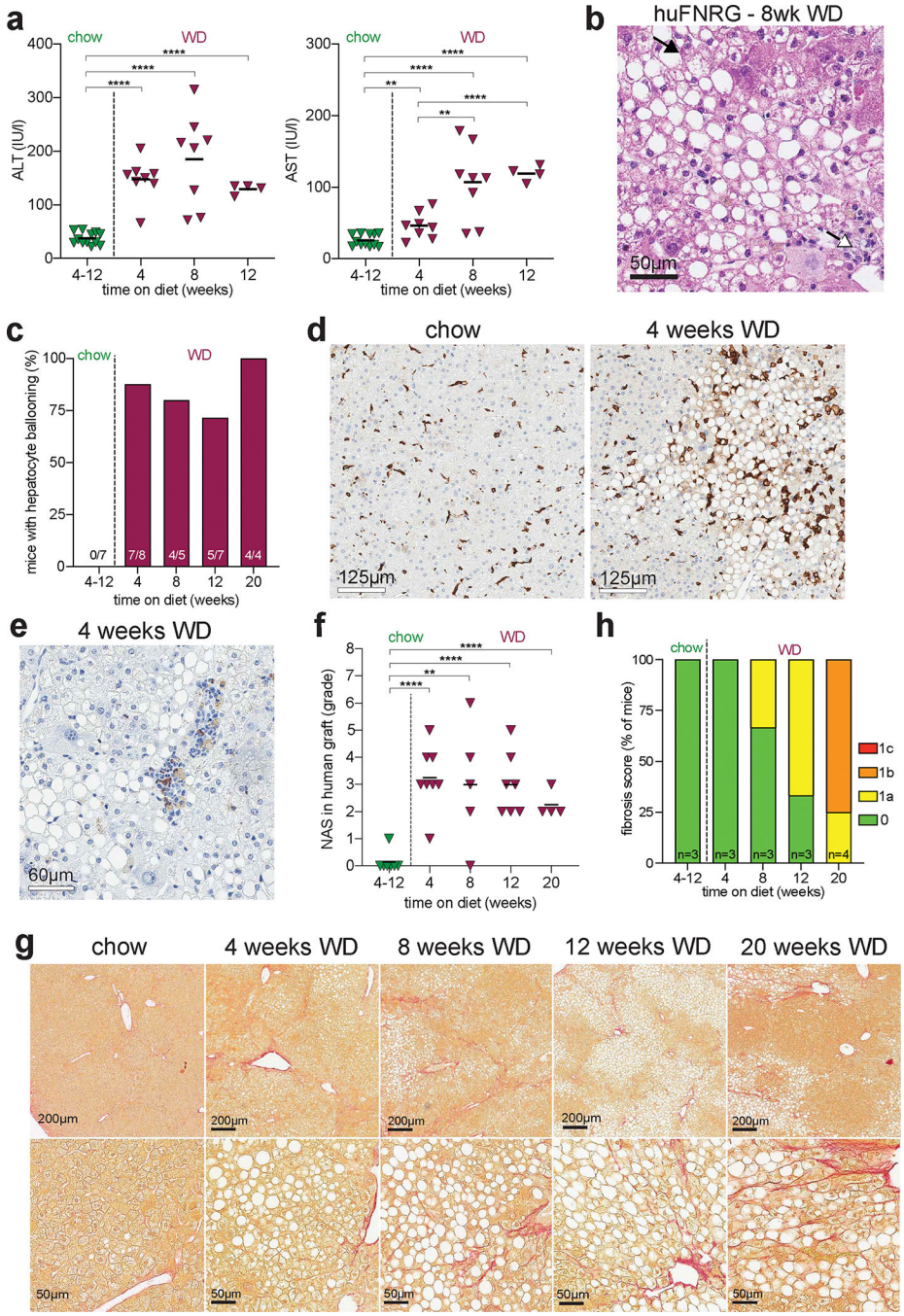

Figure 3: huFNRG mice on WD develop mild steatohepatitis.

a) ALT and AST activity in serum from huFNRG mice on chow and after 4 to 12 weeks on WD. Symbols individual mice, bars are median, unpaired *t*-test **p<0.005, ****p<0.0001.

b) H&E staining from a huFNRG mouse liver after 8 weeks on WD. Black arrow indicates hepatocyte ballooning degeneration and white arrow indicates lobular inflammation.

c) Fractions of huFNRG mice with human hepatocyte ballooning degeneration on chow and WD over time. Number of mice with ballooning per group at bottom of bars.

Author Manuscript Author Manuscript Author Manuscript Author Manuscript

d) Staining against murine macrophage marker F4/80 in the liver of a huFNRG mouse on chow and after 4 weeks of WD.

e) Staining against lymphocyte antigen 6 complex locus G6D (LY6G) in the liver of a huFNRG mouse after 4 weeks of WD.

f) NAFLD activity score (NAS) in the human graft of huFNRG mice on chow and after 4 to 20 weeks on WD. Symbols individual mice, bars are median, unpaired *t*-test **p<0.005, ****p<0.0001.

g) Picosirius Red staining for collagen in livers from huFNRG mice on chow and after 4 to 20 weeks on WD.

h) Fibrosis stages in the human graft of huFNRG liver on chow and after 4 to 20 weeks on WD. Mouse numbers at bottom of bars.

Author Manuscript Author Manuscript Author Manuscript Author Manuscript

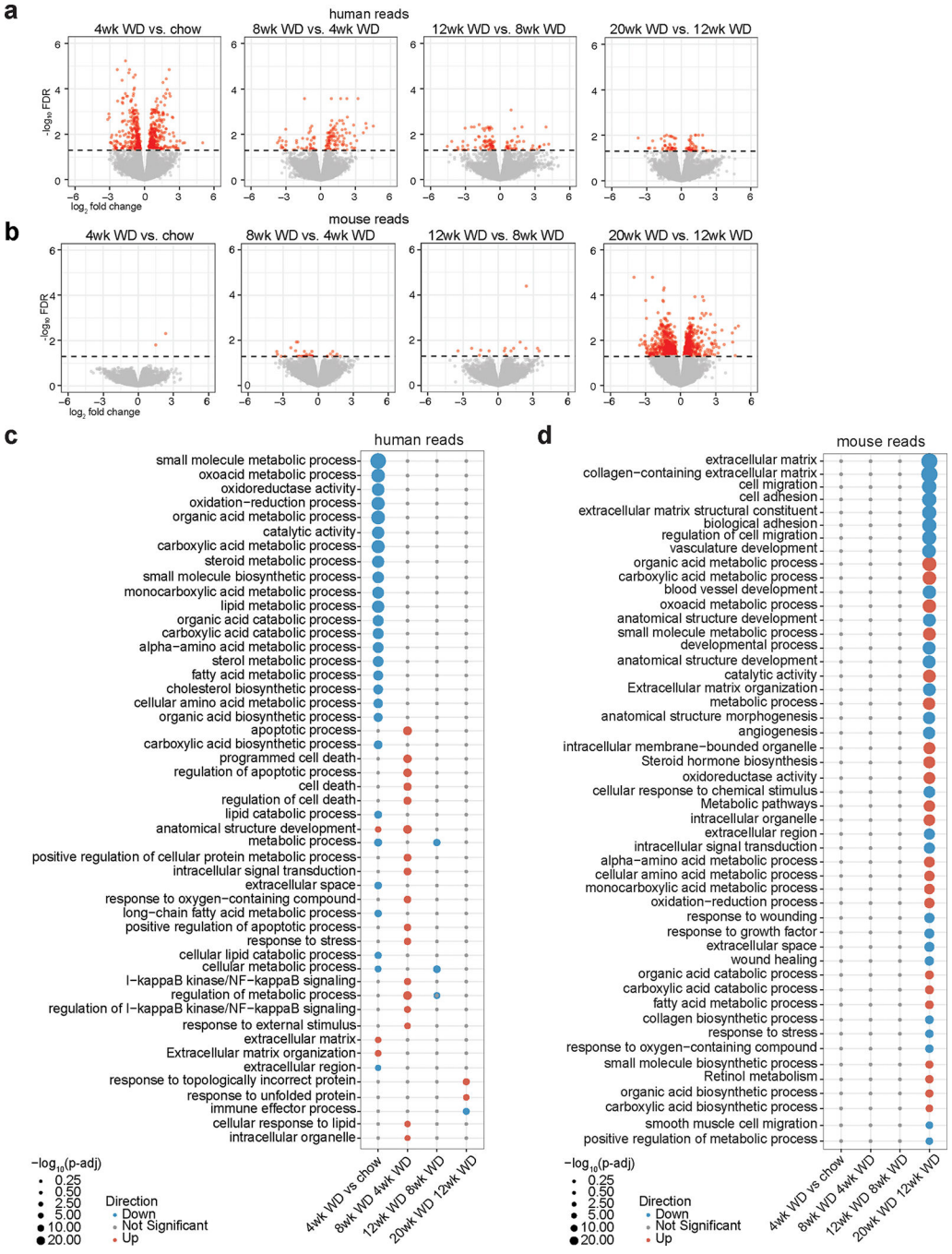

Figure 4: Transcriptional changes in huFNRG mice on WD.

a) Volcano plots of liver transcripts mapped to human genome (human reads) comparing huFNRG mice 4 weeks on WD to chow, and longer WD durations to the previous WD timepoint. RNA-sequencing of 3–4 mice per group, red symbols FDR <0.05, grey denotes not significant.

b) Volcano plots of liver transcripts mapped to mouse genome (mouse reads) comparing huFNRG mice 4 weeks on WD to chow, and longer WD durations to the previous WD

Author Manuscript Author Manuscript Author Manuscript Author Manuscript

timepoint. RNA-sequencing of 3–4 mice per group, red symbols FDR <0.05, grey denotes not significant.

c) Gene-ontology (GO) pathway analysis of human reads from livers of huFNRG mice 4 weeks on WD to chow, and longer WD durations to the previous WD timepoint. Blue symbols are down- and red symbols are upregulated pathways, grey denotes no significant changes, symbol size indicates statistical significance.

d) Gene-ontology (GO) pathway analysis of mouse reads from livers of huFNRG mice 4 weeks on WD to chow, and longer WD durations to the previous WD timepoint. Blue symbols are down- and red symbols are upregulated pathways, grey denotes no significant changes, symbol size indicates statistical significance.

Author Manuscript Author Manuscript Author Manuscript Author Manuscript

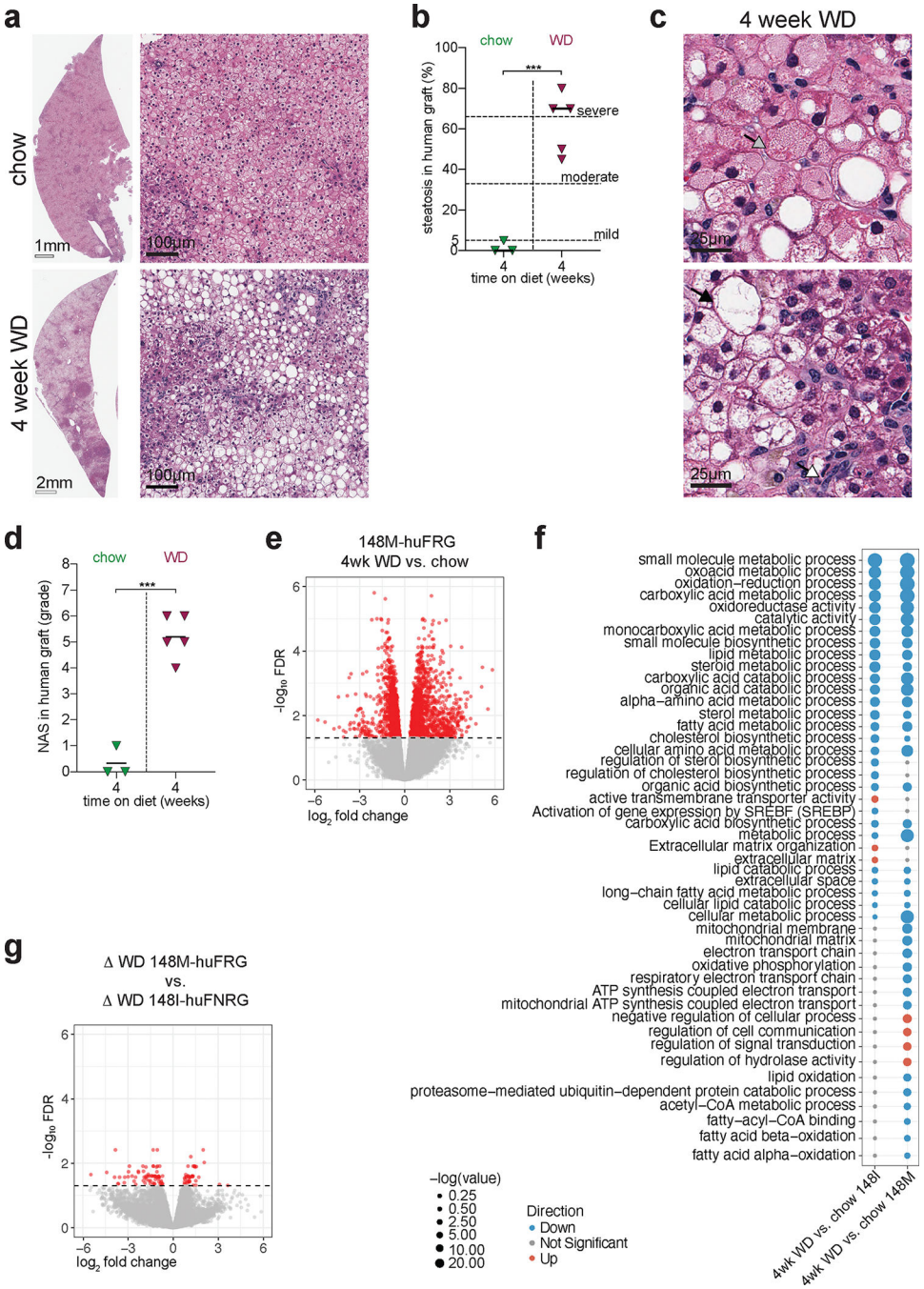

Figure 5). PNPLA3-148M huFRG mice on WD develop steatohepatitis.

a) H&E staining on livers from 148M-huFRG mice on chow and after 4 weeks on WD.

b) Clinical steatosis score of the human graft on livers from 148M-huFNRG mice on chow and after 4 weeks WD. Symbols are individual mice, bars median, unpaired *t*-test ***p<0.0005.

c) H&E staining on livers from 148M-huFRG mice 4 weeks on WD. Grey arrow indicates Mallory Denk body, black arrow ballooning degeneration and white arrow lobular inflammation.

Author Manuscript Author Manuscript Author Manuscript Author Manuscript

d) NAFLD Activity Score (NAS) in the human graft of 148M-huFRG mice on chow and after 4 weeks WD. Symbols individual mice, bars are median, unpaired *t*-test ***p<0.0005.
e) Volcano plots of liver transcripts mapped to human genome (human reads) comparing 148M-huFRG mice after 4 weeks WD vs. chow. RNA-sequencing of 3–4 mice per group, red symbols FDR <0.05, grey denotes not significant.
f) Gene-ontology (GO) pathway analysis of human reads comparing 148I-huFNRG and 148M-huFRG livers after 4 weeks WD vs. chow. Blue symbols are down- and red symbols are upregulated pathways, grey denotes no significant changes, symbol size indicates statistical significance.
g) Volcano plots of human reads differentially expressed after 4 weeks WD compared to chow (Δ WD) in 148M-huFRG livers versus 148I-huFNRG livers. Red symbols FDR <0.05, grey denotes not significant.

Author Manuscript Author Manuscript Author Manuscript Author Manuscript

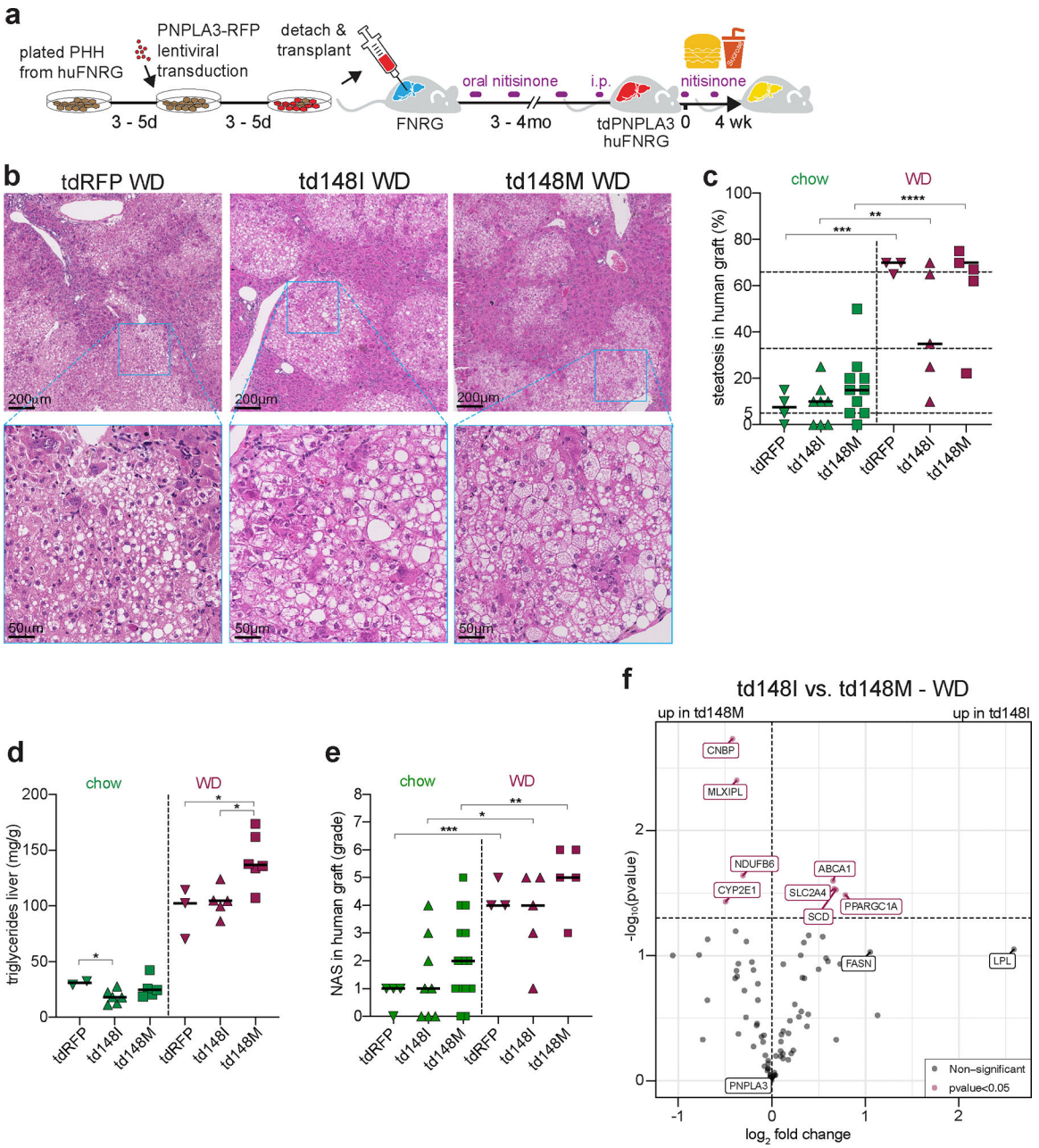

Figure 6: PNPLA3-148M overexpression in hepatocytes exacerbates steatosis in mice on WD.

a) Experimental timeline of creating PNPLA3 overexpressing mice and diet challenge. Mouse passaged primary human hepatocytes (PHH) cultures were transduced with lentiviral vectors expressing PNPLA3 variants and re-transplanted. Following humanization, huFNRG with PNPLA3 transduced hepatocytes (td) were exposed to 4 weeks of WD.

b) H&E staining on livers from tdRFP, td148I and td148M mice after 4 weeks on WD.

c) Liver steatosis score of the human graft in tdRFP, td148I and td148M mice on chow and after 4 weeks on WD. Symbols individual mice, bars are median, unpaired *t*-test with **p<0.005, ***p<0.0005 and ****p<0.0001.

Author Manuscript Author Manuscript Author Manuscript Author Manuscript

d) Hepatic triglyceride quantification in tdRFP, td148I and td148M mice on chow and after 4 weeks on WD. Symbols individual mice, bars are median, unpaired *t*-test, *p<0.05.
e) NAFLD Activity Score (NAS) in the human graft of tdRFP, td148I and td148M mice on chow and after 4 weeks on WD. Symbols individual mice, bars are median, unpaired *t*-test, *p<0.05, **p<0.005, ***p<0.0005.
f) Volcano plot of 80 human genes expressed in livers of td148I versus td148M mice after 4 weeks on WD. Expression by qRT-PCR normalized to 11 housekeeping genes, n=3–4 mice per group, burgundy symbols p<0.05, grey symbols not statistically significant.

Author Manuscript
Author Manuscript
Author Manuscript
Author Manuscript

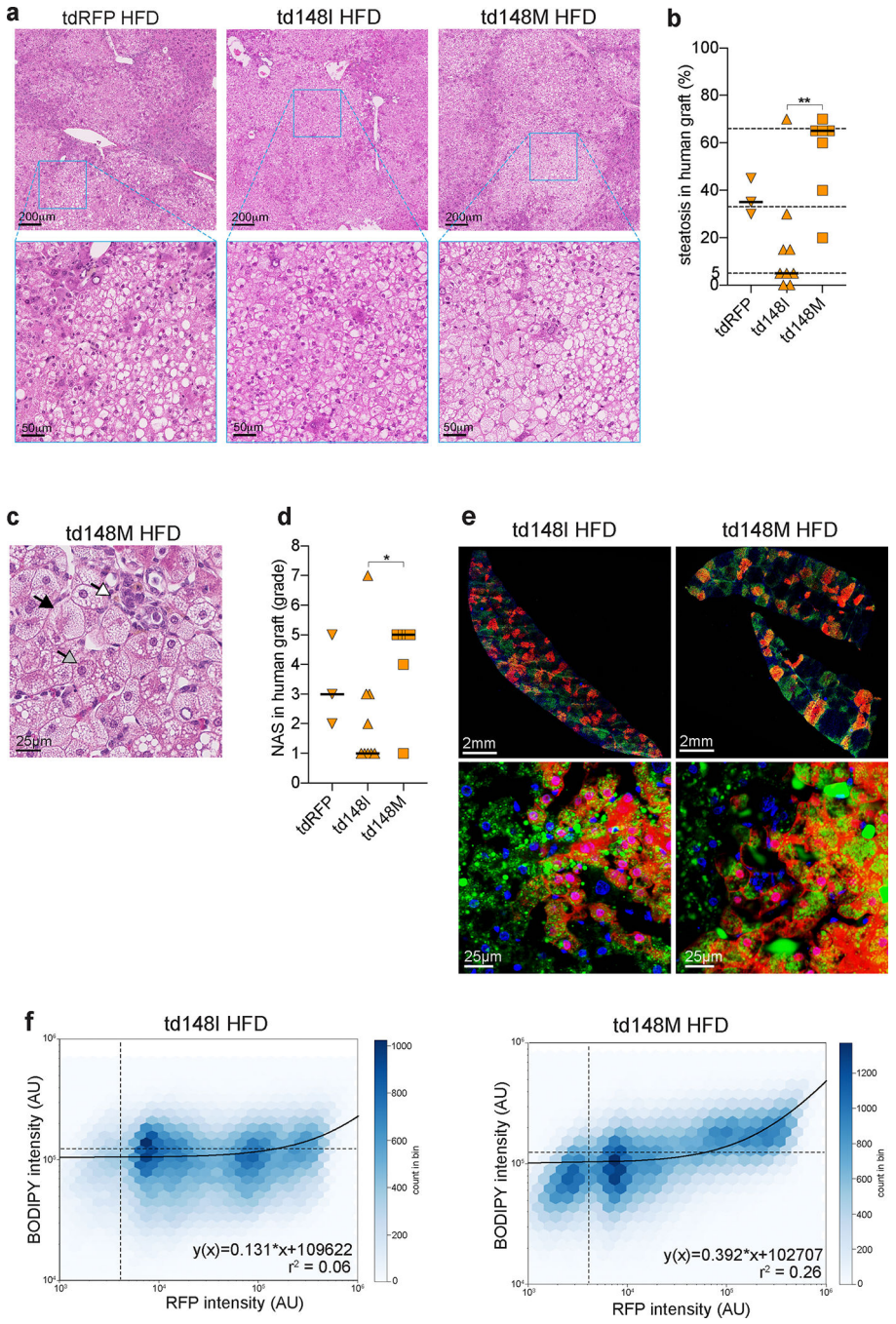

Figure 7: A HFD causes more active steatohepatitis in PNPLA3-148M overexpressing mice.

a) H&E staining on livers from tdRFP, td148I and td148M mice after 4 weeks on HFD.

b) Liver steatosis score of the human graft in tdRFP, td148I and td148M mice on chow and after 4 weeks on HFD. Symbols individual mice, bars are median, unpaired *t*-test with **p<0.005.

c) H&E staining on liver from a td148M mouse after 4 weeks of HFD. White arrow indicates lobular inflammation, black arrow microvesicular steatosis and grey arrow Mallory-Denk body.

Author Manuscript Author Manuscript Author Manuscript Author Manuscript

d) NAFLD Activity Score (NAS) in the human graft of tdRFP, td148I and td148M mice on chow and after 4 weeks on HFD. Symbols individual mice, bars are median, unpaired *t*-test, *p<0.05.

e) Low and high magnification fluorescent images of livers from td148I and td148M mice after 4 weeks of HFD stained for neutral lipids (green, BODIPY) and nuclei (blue, DAPI) and native fluorescence (red, red fluorescent protein RFP).

f) Two-dimensional density plots of neutral lipids (BODIPY) and RFP of 355,161 small hepatocytes in livers from four td148I mice and 183,289 small hepatocytes in livers from three td148M mice after 4 weeks of HFD. Density plots are displaying RFP in X-, and BODIPY intensities in Y-Axis, both in arbitrary units (AU). Dashed lines display cell population group quadrants, with lower left quadrant harboring double negative and upper right quadrant harboring double positive cells. Solid line is simple linear regression with equation displayed underneath, r^2 is Pearson correlation coefficient.

Author Manuscript Author Manuscript Author Manuscript Author Manuscript

Key sources table

REAGENT or RESOURCE	SOURCE	IDENTIFIER
Antibodies		
Human Nuclear Mitotic Apparatus protein (hNuMa)	Abcam	cat# 97585 lot# GR268490 RRID AB_10680001
Human Glutamine Synthetase (hGS)	Ventana Medical Systems Lot	lot# V0001337 RRID AB_2861318 clone GS-9
Mouse lymphocyte antigen 6 complex locus G6D (Ly-6G/6C)	Abcam	cat# 255, rat clone NIMP-R14, RRID AB_303154
Mouse F4/80	Cell Signaling	cat#70076, rabbit clone D2S9R, RRID AB_2799771
Goat Human Albumin coating for ELISA	Bethyl	cat# A80-129A
Goat Human Albumin HRP-conjugated for ELISA	Bethyl	cat# A80-229P
Bacterial and virus strains		
pSCRPSY lentiviral vector	Dr. Charles Rice, Rockefeller University	N/A
pENTR223 PNPLA3	Arizona State University	HsCD00073959 http://dnasu.org/DNASU/GetCloneDetail.do?cloneid=73959
Chemicals, peptides, and recombinant proteins		
CuRx™ Nitisinone	Yecuris	cat# 20-0028
Retrorsine	Sigma Aldrich	cat# R0382
Valganciclovir	Sigma Aldrich	cat# PHR1626-1G
Sucrose	Fisher Scientific	cat# S5-3
Glucose	Sigma Aldrich	cat# G7021
Human insulin analogue	Eli Lilly	cat# Humulin R U-100
Pyruvate	Sigma Aldrich	cat# P2256
(mp)PHH maintenance media “HCM bullet kit”	Lonza	cat# 3198
3,3',5,5'-tetramethylbenzidine (TMB)	Sigma	cat #T0440
Neutral buffered formalin	Thermo Scientific	cat# 5725
Hematoxylin	Richard-Allan Scientific	cat# 7211
Eosin	Leica	cat# 3801619
Picro Sirius Red Stain	Abcam	cat# ab150681
Masson's Trichrome Stain	Newcomer Supply	cat# 9179A
BODIPY Stain	Invitrogen	cat# D3922
Oil Red O	Sigma Aldrich	cat# O1391
Reaction Buffer for BODIPY	Ventana	cat# 950-300
ProLong™ Diamond Antifade Mountant	Invitrogen	cat# P36961
MaXtract™	Qiagen	cat# 129056
RNeasy® Mini Kit	Qiagen	cat# 74104
DNaseI	Qiagen	cat# 79254
Critical commercial assays		
Human Albumin ELISA Kit	Bethyl	cat# E88-129

Author Manuscript Author Manuscript Author Manuscript Author Manuscript

REAGENT or RESOURCE	SOURCE	IDENTIFIER
Mouse Insulin ELISA Kit	Crystal Chem	cat# 90080
ALT KIT	Elabscience	cat# E-BC-K235
AST KIT	Elabscience	cat# E-BC-K236
Human ALT ELISA KIT	Abcam	cat# ab234578
Triglyceride Kit	WAKO Diagnostics	cat #994-02891 & #994-02991
Free Cholesterol Kit	WAKO Diagnostics	cat #993-02501
Cholesterol E Kit	WAKO Diagnostics	cat #993-02601
SuperScript IV VILO	Thermo Fisher Scientific	cat# 11766050
Human Fatty Liver Array plates mRNA	Thermo Fisher Scientific	cat# 4391524
Deposited data		
Bulk RNA-sequencing raw data	NCBI Sequence Read Archive (SRA) under accession number GSE166693	https://www.ncbi.nlm.nih.gov/geo/query/acc.cgi?acc=GSE166693
Experimental models: Cell lines		
Primary Human Hepatocytes 1 (PHH1)	Lonza	cat# HUM4188
Primary Human Hepatocytes 2 (PHH2)	Lonza	cat# HUM4129
Primary Human Hepatocytes 3 (PHH3)	BD Biosciences	cat# HFCP940
Primary Human Hepatocytes 3 (PHH4)	Yecuris	cat# HHF13022
Experimental models: Organisms/strains		
Mouse: *Fah*$^{-/-}$ NOD *Rag1*$^{-/-}$ *Il2rg*^{null} (FNRG)	Dr. Charles Rice, Rockefeller University	https://doi.org/10.1073/pnas.1919035117
Mouse: *Fah*$^{-/-}$ *Rag2*$^{-/-}$ *Il2rg*$^{-/-}$ (FRG)	Yecuris	https://www.yecuris.com/frg-ko-mice/
Mouse: Thymidine kinase transgenic mice NOD SCID *Il2rg*^{null} (TK-NOG)	Taconic Biosciences	https://www.taconic.com/mouse-model/tk-nog
uPA/SCID	Dr. Philip Meuleman, Ghent University	N/A
Oligonucleotides		
Forward Primer for Sequencing PNPLA3: 5'-GCCCTGCTCACTTGGAGAAA-3		https://doi.org/10.1002/hep.23832
Forward Primer for Sequencing PNPLA3: 5'-TGAAAGGCAGTGAGGCATGG-3'		https://doi.org/10.1002/hep.23832
Software and algorithms		
Nanozoomer 2.0 HT	Hamamatsu Photonics	
FIJI	(Schindelin et al.)	https://doi.org/10.1038/nmeth.2019
NDPITools plugin	(Deroulers et al.)	https://doi.org/10.1186/1746-1596-8-92
Tools to measure RFP and BODIPY intensities in PHH of livers from chimeric mice	(Kabbani et al.)	https://doi.org/10.5281/zenodo.4531488
Python Version 3.5.10	Python™	https://www.python.org/downloads/
Prism Version 9.3.1	GraphPad	https://www.graphpad.com/scientific-software/prism/
Aperio eSlide Manager	Leica Biosystems	https://www.leicabiosystems.com/us/digital-pathology/manage/aperio-eslide-manager/

Author Manuscript Author Manuscript Author Manuscript Author Manuscript

REAGENT or RESOURCE	SOURCE	IDENTIFIER
R version 4.0.2	R Foundation for Statistical Computing	https://www.R-project.org
STAR	(Dobin et al., 2013)	https://github.com/alexdobin/STAR
g:profiler R package	(Kolberg et al. 2020)	https://biit.cs.ut.ee/gprofiler/gost
Other		
Modified PicoLab Mouse Diet 20, 0.12% Amoxicillin, irradiated	TestDiet	cat# 5058 – 5B1Q
PicoLab Rodent Diet 20	LabDiet	cat# 5053
Rodent Diet With 60 kcal% Fat, irradiated	ResearchDiet	cat# D12492i
Mouse Breeding complete feed for mice	Ssniff GmbH	cat# V1124-3
ELISA reading plates	Nunc	cat# 4424040
Blood Glucose Monitor	GE / Bionime	cat# GE100
Charged glass slides	Fisher Scientific	cat# 22-042-924